Diagnosing Southeast Tropical Atlantic SST and Ocean Circulation Biases in the CMIP5 Ensemble

Zhao Xu

Physical Oceanography Laboratory, Ocean University of China

Department of Oceanography, Texas A&M University

Ping Chang[1]

Department of Oceanography and Department of Atmospheric Sciences, Texas A&M University

Physical Oceanography Laboratory, Ocean University of China

Ingo Richter

Research Institute for Global Change, JAMSTEC, Yokohama, Japan, and Application Laboratory, JAMSTEC, Yokohama, Japan

Who Kim

Department of Oceanography, Texas A&M University

Guanglin Tang

Department of Atmospheric Sciences, Texas A&M University

[1] *Corresponding author address*: Department of Oceanography, Texas A&M University, 3146, College Station, Texas, 77840-3146
E-mail: ping@tamu.edu

ABSTRACT

Warm sea-surface temperature (SST) biases in the southeastern tropical Atlantic (SETA), which is defined by a region from 5°E to the west coast of southern Africa and from 10°S to 30°S, are a common problem in many current and previous generation climate models. The Coupled Model Intercomparison Project Phase 5 (CMIP5) ensemble provides a useful framework to tackle the complex issues concerning causes of the SST bias. In this study, we tested a number of previously proposed mechanisms responsible for the SETA SST bias and found the following results. First, the multi-model ensemble mean shows a positive shortwave radiation bias of ~20 Wm^{-2}, consistent with models' deficiency in simulating low-level clouds. This shortwave radiation error, however, is overwhelmed by larger errors in the simulated surface turbulent heat and longwave radiation fluxes, resulting in excessive heat loss from the ocean. The result holds for atmosphere-only model simulations from the same multi-model ensemble, where the effect of SST biases on surface heat fluxes is removed, and is not sensitive to whether the analysis region is chosen to coincide with the maximum warm SST bias along the coast or with the main SETA stratocumulus deck away from the coast. This combined with the fact that there is no statistically significant relationship between simulated SST biases and surface heat flux biases among CMIP5 models suggests that the shortwave radiation bias caused by poorly simulated low-level clouds is not the leading cause of the warm SST bias. Second, the majority of CMIP5 models underestimate upwelling strength along the Benguela coast, which is linked to the unrealistically weak alongshore wind stress simulated by the models. However, a correlation analysis between the model simulated vertical velocities and SST biases does not reveal a statistically significant relationship between the two, suggesting that the deficient coastal upwelling in the models is not simply related to the warm SST bias via vertical heat advection. Third, SETA SST biases in CMIP5 models are correlated with surface and subsurface ocean temperature biases in the equatorial region, suggesting that the equatorial temperature bias remotely contributes to the SETA SST bias. Finally, we found that all CMIP5 models simulate a southward displaced Angola-Benguela Front (ABF), which in many models is more than 10° south of its observed location. Furthermore, SETA SST biases are most significantly correlated with ABF latitude, which suggests that the inability of CMIP5 models to accurately simulate the ABF is a leading cause of the SETA SST bias. This is supported by simulations with the oceanic component of one of the CMIP5 models, which is forced with observationally derived surface fluxes. The results show that even with the observationally derived surface atmospheric forcing, the ocean model generates a significant warm SST bias near the ABF, underlining the important role of ocean dynamics in SETA SST bias problem. Further model simulations were conducted to address the impact of the SETA SST biases. The results indicate a significant remote influence of the SETA SST bias on global model simulations of tropical climate, underscoring the importance and urgency to reduce the SETA SST bias in global climate models.

1. Introduction

Coupled General Circulation Models (CGCMs) suffer from a prominent SST warm bias in the tropical oceans (e.g. Mechoso et al. 1995; Davey at al. 2002) and the double intertropical convergence zone (ITCZ) syndrome (e.g. Mechoso et al. 1995; Dai, 2006), which has confronted the climate modeling community for years. Specifically in the tropical Atlantic, most climate models fail to simulate a cold tongue in the eastern equatorial ocean during boreal summer in June-July-August (JJA) (Figure 1a and 1b) and many generate a reversed zonal SST gradient and too-flat a thermocline along the equator compared to observations (Davey et al. 2002) (Figure 1d). There have been many previous studies investigating the origin and causes of these biases, and different thermodynamic and dynamic processes have been proposed to explain their origin (e.g., Dewitt 2005; Chang et al. 2007; Large and Danabasoglu 2006; Richter and Xie 2008; Wahl et al. 2009; Richter et al. 2012a). Despite the insights gained by these previous diagnostic studies, little progress has been made in resolving the bias problem in the tropical Atlantic. This SST bias persists in the newly released CMIP5 ensemble (Taylor et al, 2012; see Richter et al. 2012b for an intercomparison of CMIP5 models in the tropical Atlantic). Figures 1a and 1b compare the 21-year (1984-2004) mean SST bias in the tropical Atlantic between the multi-model ensemble mean of 38 CMIP5 and 23 CMIP3 models and Figure 1c shows the SST bias difference between these two model ensembles. Evidently, the bias patterns from the previous and current generation of Intergovernmental Panel on Climate Change (IPCC) models resemble each other, indicating that the bias problem remains unresolved. In fact, compared to the CMIP3 ensemble, the severe warm SST bias off the west coast of southern Africa is worsened by approximately 1°C in CMIP5 models, although the cold SST bias in the northern tropical Atlantic is somewhat reduced, as shown in Figure 1c.

A closer examination of Figure 1 indicates that the maximum SST bias is not located on the equator, but off the west coast of southern Africa from 15°S to 25°S in the southeast tropical Atlantic (SETA) (defined by a region (5-20°E, 30-10°S) in Figure 1a), with a magnitude of more than 6°C. This bias is most pronounced along the coast and rapidly decreases in the offshore direction. Associated with the SST errors, the CMIP5 models also suffer from subsurface temperature biases, particularly along the African coast, where biases are more pronounced below than at the surface (Figure 2). Along the African coast, the maximum subsurface temperature bias is located around 17°S with an amplitude of more than 7°C. A bias of more than 6°C occupies an area extending from 16°S to 25°S in the upper 50m. Such a subsurface temperature bias is a robust feature in all models, not only CGCMs but also oceanic GCMs (OGCMs) forced with the best estimate of atmospheric surface forcing derived from observations, reanalysis or seasonal forecast models (Huang et al. 2007). While the bias magnitude is reduced in OGCMs it is still significant and the patterns in the SETA are similar (Grodsky et al. 2012). Along the equator, on the other hand, the bias in OGCMs is much smaller than that in CGCMs. The bias problem even exists in widely used ocean reanalysis data (Xu et al. 2013), such as simple ocean data reanalysis (SODA) (Carton, 2005; Carton and Giese, 2008) and hybrid coordinate ocean model reanalysis (HYCOM) (Chassignet et al., 2007). These simple comparisons indicate the persistence and intractability of the Atlantic SST bias problem, which severely undermines the credibility of climate models in simulating and projecting future climate change in the region.

The existence of the SST bias in OGCMs and ocean reanalysis datasets suggests an oceanic origin of the SETA SST bias. This is in contrast to the equatorial SST bias that is thought to be of atmospheric origin (Richter et al., 2012a; Wahl et al., 2009), in spite of the fact that the bias pattern appears to stretch continuously from the equatorial to the SETA region (Large and Danabasugolu, 2006). Compared to its counterpart in the Pacific, the ocean circulation system in the SETA has some distinctive features. The Benguela Current (BC) off the west coast of Southern Africa is driven by the surface pressure gradient associated with coastal upwelling (Peterson and Stramma, 1991) and flows equatorward from Cape Point. In contrast to the Peru Current (Humboldt Current) off the South American coast, the BC does not reach the equator, partly due to a southward coastal current, the Angola Current (AC). The AC flows against the local prevailing southerly wind and is associated with a local doming structure in the upper ocean density structure (Wacongne and Piton 1992, Yamagata and Iizuka 1995). Local wind stress curl may be crucial in determining the structure of the AC (Colberg and Reason 2006, Fennel et al., 2012). The two coastal currents converge near 16°S and form a sharp temperature front, known as the Angola-Benguela Front (ABF) (Lass et al. 2000). No such strong front is found in the southeast tropical Pacific (Penven et al. 2005). Xu et al. (2013) proposed that the failure of climate models to realistically simulate the ABF is a major cause of the warm SST bias in the region.

The southeast Pacific and Atlantic both feature extensive regions of low-level marine stratus clouds that form over the cold SST. It has been a long-standing problem that climate models underestimate low-level stratus clouds in these two regions, resulting in too much solar radiation reaching the ocean surface and a warm SST bias (Ma et al., 1996; Yu and Mechoso, 1999; Gordon et al. 2000; Huang et al., 2007; Hu et al., 2008; Chang et al. 2007). Considerable progress has been made in the past decade to understand marine boundary layer clouds and their interactions with the ocean-atmosphere-land system over the southeast tropical Pacific. The Variability of American Monsoon Systems (VAMOS) Ocean-Cloud-Atmosphere-Land Study (VOCALS) program (Mechoso and Wood, 2010; Mechoso et al. 2014 and references therein) and the preceding Eastern Pacific Investigation of Climate Processes in the Coupled Ocean – Atmosphere System (EPIC) program (Bretherton et al. 2004) have resulted in a substantial body of knowledge on the southeast Pacific stratocumulus deck and its effects on climate model biases, as well as invaluable atmospheric and oceanic observational data sets to understand and validate climate model simulations (de Szoeke and Xie, 2008). Studies within these programs further support the notion that stratocumulus cloud decks are a major factor in the climate model biases in the southeast tropical Pacific. Among these studies is a model-data comparative analysis by de Szoeke et al. (2010) that compared an ensemble of CMIP3 model simulations to various observations in the southeast Pacific stratocumulus deck region. Their results reveal that all CMIP3 models have at least 30 Wm^{-2} too much solar warming in October due to poorly simulated stratus clouds. These findings of VOCALS and EPIC programs can be extremely valuable in understanding the tropical Atlantic bias and motivate us to quantify the role of the stratocumulus cloud decks in the SETA SST bias. Given the distinct ocean circulation features in the SETA region as discussed above, we would like to know the relative importance of the stratus-cloud induced shortwave radiation error in comparison with other systematic errors of oceanic origin in causing the SETA SST bias.

In contrast to the southeast tropical Pacific region, the SETA stratocumulus cloud process and the associated ocean-atmosphere-land interactions are less understood and direct field observations are scarce in the region. A few existing studies are largely model-based and somewhat inconclusive. Huang et al. (2007) used the NCEP coupled forecast system (CFS) model to study the initial bias growth and concluded that the inability of CFS to reproduce realistic amounts of low clouds in the SETA is a major cause of the warm SST bias. Hu et al. (2008) later found that the underestimation of the low cloud with the same model stemmed from the cloud scheme employed in the atmospheric model. However, Large and Danabasugolu (2006) argued that the solar radiation bias was not enough to generate a 5°C warm SST bias. A similar conclusion was also drawn by Wahl et al. (2009) in their investigations with the Kiel climate model. By artificially reducing the shortwave radiation at the ocean surface in their model, they found that the warm SST bias was reduced by approximately 50%, but not eliminated. Besides the direct warming effect, possible thermodynamic and dynamic feedbacks may exist between low clouds and SST. For example, Nigam (1997) proposed that in the southeast tropical Pacific insufficient low clouds in climate models reduces longwave radiation heat loss at cloud-top, which in turn can induce weakened subsidence and reduce near-surface divergence. In the southeast tropical Pacific, this weakened divergence causes a northerly wind anomaly along the coast, leading to weakened coastal upwelling and warmer SST.

From an oceanic perspective, the BC region is one of the strongest coastal upwelling regions in the world oceans. Driven by the alongshore southerly winds, the off-shore Ekman flow induces an upward vertical flow and brings cold deep ocean waters to the surface. The warm bias in models is possibly due to insufficient coastal upwelling (Large and Danabasugolu, 2006). Indeed, Huang (2004) found that the alongshore winds were too weak to generate adequate coastal upwelling in the COLA CGCM. Wahl et al. (2009) suggest that insufficient resolutions in current generation CGCMs may be a potential cause for the upwelling problem. Seo et al. (2006) showed a reduced SST bias along the African coast by only increasing the ocean model resolution in a regional coupled model simulation. They attributed this SST bias reduction to the improvement in simulating oceanic meso-scale activity and coastal upwelling. Similar improvements due to enhanced model resolution are also found in two different versions of the GFDL coupled model (Doi et al., 2012). However, Kirtman et al. (2012) did not find any significant improvement of the SETA SST bias when they increased the ocean model resolution from 1° to 0.1°.

Two independent GCM studies by Richter et al. (2012a) and Wahl et al. (2009) found that an improved simulation of the deep tropics can lead to a reduction in the SETA SST bias by 2~3°C, without changing the local surface forcing. This reduction, however, is not strong enough to eliminate the warm SST bias that is on order of 5-6°C. Richter et al. (2012a) speculated that the equatorial influence was mediated through Kelvin waves propagating along the equatorial and coastal waveguides. A recent study by Toniazzo and Woolnough (2013), based on an error growth analysis of three CMIP5 model decadal hindcast experiments, also highlighted the importance of the remote influence of equatorial SST errors on SETA SST errors via subsurface ocean anomalies. In the long-term mean sense, the AC flows southward along the African coast, so the SST bias in the eastern equatorial Atlantic could be advected to the SETA region by the AC.

Regardless which one of these mechanisms dominates, these studies suggest that the biases along the equator and in the SETA are linked to a certain extent.

All the above-described mechanisms are likely to contribute to the SETA SST bias, but their relative importance has not been fully determined. This study attempts to quantify the relative contribution from each of these proposed mechanisms to the warm SST bias in the SETA using the latest CMIP5 ensemble. In section 2, we will first describe the CMIP5 data set along with observed and reanalysis data sets used to validate the model simulations. In section 3, we will examine each of the proposed mechanisms for the SETA SST bias by analyzing the CMIP5 data set against observed and reanalysis datasets. In section 4 and 5, we will focus on examining the oceanic mechanism suggested by Xu et al. (2013) that identifies the oceanic advection as a key process responsible for the strong warm SST bias in the SETA. In section 6, we attempt to address the climate impact of the SETA SST bias. Finally, in section 7 we will summarize major findings of this study.

2. Datasets

In this section, we give a brief description of various modeling and observed data sets used in this study.

2.1 CMIP5 model ensemble

The CMIP5 multi-model ensemble includes a set of CGCM simulations carried out by various modeling centers and groups around the world to understand past and future climate change, forming the basis of IPCC fifth assessment report (AR5; Taylor et al., 2012). In this study, we chose 38 models for our analysis and a brief description of these is given in Table 1. We use CMIP5 hindcasts of the 20th century, which employ the observed historical greenhouse gas and other external forcings and cover the period from 1870 to 2005 (this integration period varies in some model runs). To compare the CMIP5 model ensemble to its predecessor, CMIP3, we also analyzed 23 CMIP3 models' 20th century climate simulations (20C3M) for the same time period as CMIP5. To assess the role of coupled surface flux feedbacks, we also examine experiment AMIP in the CMIP5 archive, in which models are forced with observed SST.

2.2 Reynolds SST

The optimally interpolated (OI) Reynolds SST with a daily temporal resolution and 0.25° spatial resolution is used as the observed SST to validate the model simulations. The data set is based on in-situ observations, National Oceanographic Data Center (NODC)'s Advanced Very High Resolution Radiometer (AVHRR) Pathfinder Version 5 satellite measurements from September 1, 1981 to December 31, 2005, and the operational US Navy AVHRR data from January 1, 2006 to present. It includes a bias correction of the satellite data in reference to in situ observations using an Empirical Orthogonal Teleconnection (EOT) algorithm (see Reynolds et al., 2007 for more details).

2.3 NCEP-CFSR

The National Centers for Environmental Prediction (NCEP) Climate Forecast System Reanalysis (CFSR) (Saha et al., 2010) is a recently released reanalysis dataset. It is based on a global high-resolution coupled ocean-atmosphere system. Its atmospheric component has a spectral resolution of T382 (~38 km) and 64 vertical levels, and its oceanic component has a uniform grid of 0.25° in longitude, a meridional grid varying from 0.25° at the equator to 0.5° outside tropics, and 40 vertical levels.

2.4 OAFlux

The Objectively Analyzed air-sea Flux (OAFlux) data set is derived from satellite data, in-situ observations and Numerical-Weather-Prediction (NWP) reanalyses using bulk parameterizations. This product provides daily air-sea fluxes on a 1° grid covering the global oceans that validated against buoy data (Yu and Weller, 2004).

2.5 COREII

Coordinated Ocean-ice Reference Experiments version 2 (COREII) dataset is the descendent of COREI, providing a common interannual forcing field for ocean-ice simulations. It combines satellite measurements with reanalysis datasets with an improved algorithm to derive the surface fluxes. The data set contains interannually varying surface variables from 1948 to 2007 with 6-hourly temporal resolution for some variables, such as winds. More details can be found in Large and Yeager (2004, 2008).

2.6 POP Simulation

The Parallel Ocean Program (POP) was developed at the Los Alamos National Laboratory (LANL). It solves the 3-dimenional primitive equations under the hydrostatic and Boussinesq approximations and employs a z-vertical coordinate and finite-difference discretization method for the spatial derivatives. In this study we analyze simulation results of POP version 2 (POP2) forced with 60-year (1948-2007) COREII surface forcing to compare them with the results from CCSM4, which uses the same POP2 as its oceanic component. It has a nominal 1° horizontal resolution on a curvilinear grid with the North Pole displaced over Greenland. The layer thickness between the 60 vertical levels varies from 10 m in the upper 160 m, to 250 m near the bottom. A detailed discussion of model physics parameterizations is provided by Danabasoglu et al. (2012). The simulation was run for 14 cycles (840 years) (Table 2) to allow the model to reach equilibrium and the last cycle was used for our analysis to minimize the errors from potential model drift. By comparing POP2 and CCSM4 simulations, we attempt to distinguish between biases originating in the oceanic and atmospheric components of the coupled model.

Unless noted otherwise, a 21-year period from January 1984 to December 2004, which is the common period of all the datasets listed above, was chosen for the bias analysis. In the POP simulation, the field from 1984 to 2004 in the last forcing cycle is used for analysis.

3. Mechanisms of SETA SST Bias

3.1 Stratocumulus Cloud and Shortwave radiation

A common problem in CGCMs is the under-representation of stratocumulus decks in the SETA region, which leads to excessive shortwave radiation at the ocean surface (Huang et al., 2007 and Hu et al., 2008). However, Large and Danabasugolu (2006) argued that the bias due to shortwave radiation is too small to account for the severe warm SST biases in the region, which often exceed 5 K. Figures 3a and 3c show shortwave radiation in the OAFlux data and the CMIP5 ensemble. In the following discussion, positive is defined as heat flux into the ocean. Shortwave radiation is conspicuously low in the area 0-10°E and 20-10°S in OAFlux, consistent with shortwave reduction due to the presence of stratus cloud. Clearly, this region of low shortwave radiation is much less prominent in the CMIP5 ensemble. Apart from reflecting incoming shortwave radiation, stratocumulus cloud also reflects ocean-emitted longwave radiation back to the surface and thus reduces ocean heat loss. As a result, the influence of stratocumulus is not only visible in the shortwave fluxes (Figure 3a) but also in the longwave fluxes (Figure 3b) in OAFlux. In the CMIP5 ensemble, on the other hand, this signature of the stratocumulus is much less pronounced. CMIP5 models also show excessive shortwave radiation along the African coast compared to OAFlux (Figure 3c), coinciding with the maximum SST bias in the same region as shown in Figure 1a.

In addition to shortwave and longwave radiation, sensible and latent heat fluxes are also crucial to the net surface heat flux. To quantify their contributions to the net surface heat flux, we average these fields over all the ocean points within two areas, (5-20°E, 30-10°S) and (5°-10°E, 25-10°S), respectively. The first region covers the area of maximum SST bias (see the box in Figure 1a) and its choice is motivated by the desire to identify the cause of the SST bias, which is the main objective of this study. We will use this area for all the following area-averaged analyses unless otherwise noted. However, this region is not necessarily well suited to study the effect of the main SETA stratocumulus deck. This deck is located off the coast (Figure 3) due to a low-level atmospheric jet along the Benguela coast (Nicholson, 2010), which can clear much of the cloud in the region, as indicated in Figure 3. Due to the presence of the jet, oceanic processes can become more dominant in the local heat budget, making it difficult to assess the importance of the SETA stratocumulus deck in model biases. To address this issue, we define a second area that covers the area of maximum SETA stratocumulus incidence (marked by a box in Figure 3a).

The results of the surface heat flux analysis are shown in Figure 4. In the SETA region, Figure 4a clearly shows that the shortwave radiation is the only positive flux and that it dominates the net surface heat flux. In fact, the shortwave radiation is greater than the sum of the other three components in both CMIP5 and OAflux, so that the net heat flux has the same sign as the shortwave radiation. This indicates that the atmosphere tends to warm the ocean surface in the SETA.

There are, however, large discrepancies between heat fluxes derived from CMIP5 and OAflux. Shortwave radiation is excessively large in CMIP5, resulting in a positive flux bias of about 20 Wm^{-2}. The dominant bias, however, is that of the latent heat flux, which is on the order of 50 Wm^{-2} compared to OAflux, followed by the longwave radiation bias. Both of these fluxes are overestimated in the CMIP5 models, thus offsetting the shortwave radiation bias. As a result, the net surface heat flux bias is negative, indicating that the ocean receives considerably less net surface heat flux (~60 Wm^{-2}) in the models than in observations. This seems to suggest that the heat flux bias should result in a cold SST bias in this region in the absence of other processes. One has to consider, however, that the underlying SST is quite different in CMIP5 and OAflux, which likely influences the flux balance.

To estimate the influence of the warm SST bias on the surface fluxes, we examine an ensemble of atmosphere-only GCMs forced with observed SST (experiment AMIP in the CMIP5 archive; see Table 1 for a list of ensemble members). The analysis suggests that the presence of the warm SST bias leads to an increase of latent heat flux by about 30 W m^{-2}. The influence is less pronounced for longwave and shortwave radiation, which only increase by ~3 and ~2 W m^{-2}, respectively. Notwithstanding the impact of SST biases on the flux balance, it is obvious that even in the AMIP ensemble the net flux into the ocean is smaller than in OAflux data, resulting in a negative net surface heat flux bias of approximately 30 Wm^{-2}. We further note that the shortwave flux into the ocean increases by less than 2 W m^{-2} in CMIP5 relative to AMIP, suggesting a weak stratocumulus-SST feedback in CMIP5 models.

However, as mentioned earlier, the presence of the low-level atmospheric jet in the SETA region may lessen the effectiveness of the stratocumulus cloud error in generating SST biases. We next examine the same heat flux analysis in the main stratocumulus deck region (see the box in Figure 3a). The result shows that although the shortwave radiation biases in both CMIP and AMIP do increase by ~20-30% compared to the value in the SETA region, consistent with the large model biases in simulating stratocumulus cloud in the region, these increases are not sufficiently large to change the sign of the net surface heat flux biases and they remain to be negative even in the main SETA stratocumulus region (Figure 4b). As a result, the net heat flux biases in both CMIP and AMIP behave similarly to those in the SETA region (Figure 4a). Since a positive net heat flux is defined as into the ocean, the negative net heat flux biases indicate that less heat is pumped into the ocean in the models than in reality even under the main SETA stratocumulus deck, acting to cool but not warm the ocean, despite the increased shortwave radiation error. de Szoeke et al. (2012) reported a 40 Wm^{-2}

shortwave radiation bias in the CMIP3 ensemble over the main southeast tropical Pacific stratocumulus deck region, which is sizably larger than the shortwave radiation bias (~25 Wm^{-2}) we found over the SETA stratocumulus deck region in the CMIP5 ensemble. This difference is consistent with the notion that the Pacific stratocumulus deck is a more dominant player in the southeast tropical Pacific SST bias than its Atlantic counterpart.

Figure 5 and 6 show spatial maps of the flux biases for the individual heat flux components and their sum, respectively. As shown in Figure 5, except shortwave radiation all flux components show biases that remove too much heat from the ocean. The strip of excessive shortwave radiation along the coastline mentioned earlier (Figs. 3c and 5a) is compensated by the sensible and latent heat fluxes. As a result, the CMIP5 net surface heat flux is less than the observationally derived OAflux value over the SETA region, with a maximum negative bias of over 100 $Watts/m^2$ near the region where the SST bias is strongest (Figure 6). This finding is consistent with the argument that the warm SST bias is caused by oceanic mechanisms, while the atmospheric fluxes tend to damp the warm bias by removing excessive heat from the ocean. We note that the net surface heat flux bias shown in Figure 6 acts to cool the ocean everywhere within the tropical Atlantic, including the entire SETA stratocumulus deck region where the shortwave radiation bias is positive. This explains the insensitivity of the surface heat flux analysis to the choice of averaging region, as demonstrated by Figure 4a and 4b.

We further analyze the role of surface heat flux biases in a scatter plot of SST versus net surface heat flux biases over the SETA region for the CMIP5 models (Figure 7a). The average SST bias in this region ranges from 1º to 5ºK and the net heat flux bias ranges from -50 to -80 Wm^{-2}. If surface heat flux biases were largely responsible for the

SST biases and other causes are not important, one would expect a significant correlation between the two quantities, because a model with a larger heat flux bias should produce a bigger SST bias and vice versa. This is clearly not the case. In fact, a linear fit shows a nearly horizontal line and the correlation between the two quantities is essentially zero, indicating that the SST bias is not related in any simple way to heat flux biases.

3.2 Coastal Upwelling

Poorly simulated coastal upwelling in CGCMs is another widely discussed potential cause of the warm SST biases (Large and Danabasugolu, 2006). The BC region is one of the most prominent upwelling regions in the world oceans. The prevailing surface winds along the coast drive offshore Ekman transport and divergence along the coast. Upwelling of deep and cold subsurface water compensates the water mass loss at the surface and cools the surface ocean. Figure 7b shows the relationship between the inter-model vertical mass transport (in kg s^{-1}) and SST bias. Because only a subset of the CMIP5 ensemble provides the vertical mass transport, 20 CMIP5 models were used in the scatter plot. The vertical mass transport, taken at 50 m below the sea surface, is averaged within a 3° wide band along the coast from 15°S to 30°S. The resultant correlation is 0.14, which is low and statistically insignificant. The absence of a linear inter-model relationship between SST biases and coastal upwelling indicates that the SST bias is not simply determined by model upwelling error, i.e., a stronger deficiency in simulated upwelling does not translate to a more severe warm SST bias. It is worth noting that the correlation coefficient is not sensitive to the width of the coastal band used to average the vertical mass transport and the depth at which the vertical mass transport was taken (50m). Using a 5° wide band and/or vertical mass transport at 100m yields a similar result.

To further investigate the role of coastal upwelling in SETA SST bias, we correlated alongshore wind stress and vertical mass transport within the model ensemble and obtained a correlation of ~0.49, which is significant at the 95% level (Figure 8a). The alongshore wind stress is defined as the modulus of the wind stress projected onto an angle of 68° relative to parallels and averaged within the same region as vertical mass transport. The high correlation indicates that the strength of the simulated upwelling by CMIP5 models is related to the strength of the alongshore winds. Furthermore, the correlation between alongshore winds and SST biases is 0.47 (Figure 8b), which is significant at the 95% level. The correlation analyses imply that the SST bias is affected by the simulated alongshore winds, but not simply through upwelling-induced vertical heat advection. Other oceanic processes, such as horizontal advection, which are affected by the local winds and coastal upwelling, may play a more important role in SETA SST bias.

South of the ABF region, the wind-driven coastal upwelling maintains a pressure gradient pointing toward the coast that drives the northward BC and transports cold water northward. It is conceivable that a weak alongshore wind can lead to a weakened BC, resulting in surface warming near the ABF, owing to deficient cold-water transport from the south. Because of the strong meridional SST gradient near the ABF, failure to accurately represent coastal currents can result in large errors in horizontal heat advection, which may be more dominant than vertical heat advection in balancing the local oceanic heat budget of the region. As such, the Benguela coastal upwelling error in

CMIP5 models can indirectly contribute to the SST bias via its impact on horizontal heat advection. We will return to this discussion in the following section.

3.3 Remote Influence From Upstream

Richter et al. (2012a) and Wahl et al. (2009) performed numerical experiments in which they replaced the model surface winds with observed winds between 1°S and 1°N (Richter et al., 2012a) and 4°S and 4°N (Wahl et al., 2009). As a result, the simulated equatorial SST was improved, which helped to reduce the SST bias in SETA by about 30%. This indicates that some of the SETA SST errors originate upstream in the AC, either through advection or Kelvin wave propagation toward the SETA. Toniazzo and Woolnough (2013) also identified a robust connection between the Atlantic equatorial temperature errors and SST errors along the Benguela-Angola coast. Although this upstream effect is unlikely to be fully responsible for the SETA SST bias, because upstream temperature biases are typically less severe than the SETA SST bias, its contribution may still be significant.

To quantify this remote contribution, we analyzed the relationship between SST biases over the southeastern equatorial-Atlantic between 0°-15°E and 10°S to 0° and SST biases over the SETA region. The scatter plot shown in Figure 7d indicates a positive correlation of 0.48, which is significant at the 95% level based on a student t-test. We note that the equatorial SST biases are weaker than those in the SETA region. Furthermore, since the equatorial undercurrent (EUC) is also one of the sources for the AC (Wacongne and Piton 1992), the temperature bias in the equatorial thermocline is also expected to have an influence on the SETA SST bias. Figure 7c shows a scatter plot of CMIP5 model equatorial thermocline temperature biases averaged over an area between 5°W-10°E and 2°S-2°N and a depth range between 20m-100m, where the equatorial subsurface warm bias is strongest, against the SST biases in the SETA. The correlation coefficient is nearly 0.33, indicating that the thermocline temperature bias may make an important contribution to the coastal SST bias. However, we note again in that the thermocline temperature biases with a mean bias of about 2 °C are weaker than the coastal SST biases that have a mean value of about 3 °C. To further validate the remote influence of the equatorial biases on the coastal biases, we performed a lag correlation analysis of the monthly multi-model ensemble mean biases (not shown). Results indicate that on average the equatorial thermocline bias leads the SETA SST bias by about one month in CMIP5 models, suggesting that it is the equatorial temperature bias that affects the SETA SST bias.

The above analyses indicate that the SETA warm SST bias is more likely related to systematic errors in dynamic processes, both local and remote ones, than to thermodynamic processes in CMIP5 models. The discussion in section 3.2 further points to the potentially dominant role of horizontal ocean heat advection in causing the warm SST bias near the ABF. However, none of the dynamic mechanisms described above directly relate the SETA SST bias to the erroneous southward shift of the ABF. This southward shift is likely to be important because the center of the SETA SST bias is clearly co-located with the ABF, as shown Figure 1. Motivated by this observation, in the next section we further explore the relationship between the ABF location and the SETA SST bias.

4. Mechanism Linking SETA SST Bias to ABF Location Error

The ABF is characterized by strong near surface convergence and a strong meridional SST gradient. However, due to the lack of sufficient direct measurements of the surface current field, it is difficult to use direct observations to validate CMIP5 model simulations. Instead, we will use currents derived from the NCEP/CFSR reanalysis as a reference. We choose NCEP/CFSR because among all the ocean reanalyses we examined, it compares most favorably to the few existing hydrographic measurements in the ABF region (e.g., Lass et al. 2000). In particular, NECP/CFSR reproduces the strong meridional temperature gradient associated with the ABF and reproduces its observed latitude at around 16°S (Lass et al. 2000). As shown in Figure 9a and 10b, at the front the two coastal currents, the AC and the BC, converge, resulting in a westward off-shore flow. The subsurface core of the AC shown in Figure 10 is likely related to the local wind stress curl (Fennel et al. 2012). South of the ABF and off the coast of Namibia, the BC decays rapidly off the coast, indicating the role of coastal upwelling. In the multi-model ensemble mean of CMIP5 model simulations, however, near surface currents converge at 25°S (Figure 9b) and the northward velocity is also considerably weaker than that in NCEP/CFSR, indicating a very weak BC in the models. This flow structure is consistent with the notion that the upwelling in CMIP5 is too weak, resulting in a very weak BC, as discussed in section 3.2.

The weak BC in CMIP5 model simulations partially explains the southward displacement of the ABF because it enables the AC to overshoot across the observed ABF latitude and transport warm and saline water to the latitudes of the observed Benguela upwelling zone. We therefore hypothesize that the overshoot of the AC and the associated southward heat transport are a major cause for the warm SST bias in the SETA. This mechanism offers an explanation as to why the maximum warm SST bias in CMIP5 models is located near the ABF.

We test this hypothesis by first examining the relationship between simulated ABF locations and SETA SST biases in all CMIP5 models. If the hypothesis is valid, we expect to see a significant positive correlation between these two quantities, because a larger southward shift of the ABF should imply a stronger AC overshoot and thus stronger southward heat advection. Figure 11 shows a scatter plot between ABF location and SST biases in all CMIP5 models. Here the ABF location is defined as the latitude where the zonally averaged meridional velocity within 3 degrees along the coast vanishes and the SST bias is averaged between 5°E-20°E and10°S-30°S. The correlation coefficient of these two quantities is 0.66, which not only passes the 99% significance level of the student t-test, but is also higher than all other correlation values discussed in Section 3. Therefore, multi-model analyses of CMIP5 data seem to support the hypothesis that the overshoot of the AC is a primary cause for the warm SST bias in the SETA region.

The next question is what physical processes cause the overshoot of the AC and the southward displacement of the ABF in CMIP5 models. The fact that all CMIP5 models show a southward shift of the ABF by 3° to 15° (Figure 11) suggests that there may be common cause for this bias. Since the ABF is maintained by the relative strength of the AC and the BC (Colberg and Reason, 2006), the cause should be related to the physical factors that influence the strength of these currents.

We begin by examining the vertical temperature profile along the African coast. In NCEP/CFSR, the strong horizontal temperature gradient near 16°S (Figure 2b) is clearly maintained by the two opposing currents, the AC and the BC, as shown in Figure 10b. The difference in thermal structures on two sides of the front is striking. North of the front the thermocline is sharp and forms at a shallow depth of around 50m while SST is warm (Figure 2b). South of the front SST is much cooler and the water column is well mixed, without a visible thermocline. In this region, the temperature contours are lifted upwards, indicative of strong upwelling (Figure 2b). In CMIP5, one sees a very different thermal structure in the Benguela upwelling region with stratified water masses extending all the way to 30°S (Figure 2a), indicating that upwelling is much weaker. The thermocline north of the ABF is too deep and too diffuse compared to the NCEP/CFSR analysis. Together, these differences suggest that the BC, whose strength is linked to the Benguela upwelling, is too weak, while the AC is too strong in CMIP5 models.

Next we examine the surface winds. Figure 12 shows the 11-year (1997 to 2007) mean surface wind stresses in CMIP5 and COREII, as well as the difference between the two. In COREII, the maximum wind stress is located just off the coast with a magnitude of more than 0.1Pa. In CMIP5 the wind stress is much weaker and its maximum strength is located farther away from the coast than in COREII. This results in a northerly wind stress bias with a maximum magnitude of more than 0.05Pa along the coast (Figure 12c). Such a northerly wind bias exists in all CMIP5 models examined in this study. The deficient alongshore southerlies in CMIP5 are largely responsible for the weak simulated coastal upwelling, and thus the weak BC, as suggested by the significant correlation between inter-model alongshore winds and vertical mass transport shown in Figure 8a

Several possible explanations for the alongshore wind bias have been proposed. Large and Danabasoglu (2006) suggested that insufficient resolution in atmospheric models can cause problems in resolving steep orography along coastal regions, particularly the Andes Mountain Range that spans the entire west coast of South America. The mountain range along the west coast of southern Africa is less steep but may still play a significant role in determining the strength of the South Atlantic high and thus the coastal winds (Richter et al. 2008). Patricola et al. (2011) show in their regional model simulations that local winds in SETA are sensitive to land surface model and convective parameterizations. Nigam (1997) propose that deficient stratocumulus in CGCMs can cause anomalous warming at the cloud top, which induces ascending motion and convergence near the ocean surface. This results in anomalous northerly winds near the coast, which can weaken the alongshore southerlies. A comparison between CMIP5 and COREII winds hints that the low-level atmospheric jet along the Benguela coast, the so-called Benguela jet (Nicholson, 2010), may not be captured by CMIP5 models. Nicholson (2010) suggests that the Benguela jet is reminiscent of the jet along the Peruvian coast (hereafter referred to as the Peruvian jet). Both regions are characterized by large-scale flow parallel to the coast, the presence of a north–south coastal mountain chain, strong coastal upwelling, and a temperature inversion at the top of the marine boundary layer. Garreaud and Muñoz (2005) and Muñoz and Garreaud (2005) investigated the dynamics of the Peruvian jet and suggested that the magnitude of the jet should be closely related to the meridional pressure gradient. We performed a simple correlation analysis between CMIP5 sea-level pressure (SLP) gradients and near-coast meridional wind stress. This analysis, however, did not yield statistically significant correlations, suggesting that the failure of CMIP5 models in simulating the Benguela jet may involve more complex dynamics. A full understanding of this issue requires a comprehensive analysis of momentum budget in CMIP5 models, which is beyond the scope of this study.

Furthermore, the local surface wind stress can affect the southward extension of the AC. Colberg and Reason (2006) suggested that the local wind stress curl north of the ABF controls the ABF location. This is because the negative wind stress curl can steer the south equatorial counter current (SECC) southward by generating negative potential vorticity in the ocean. The analytical solution presented by Fennel et al. (2012) also highlights the importance of the local wind stress curl in shaping the ABF and Benguela upwelling through the interplay between the curl driven effects and the coastal Ekman upwelling. In CMIP5 models, the eastward shift of the maximum wind stress generates an excessive negative wind stress curl in this region (Figure 13), which is likely to contribute to the overshoot of the AC in CMIP5 models.

The above mechanisms suggest that the SETA warm SST bias can be attributed, to a large extent, to the erroneous local surface wind forcing. Wahl et al. (2009), on the other hand, raised the possibility that insufficient OGCM resolution may also contribute to upwelling and thus SST biases, because coastal upwelling dynamics are not properly resolved. This suggests that even if there are no biases in coastal winds, OGCMs may still produce biases in the SETA, which can be amplified by local air-sea interaction in CGCMs. In the next section, we will examine this possibility by comparing biases in a CGCM simulation to those in a stand-alone ocean-sea ice model simulation forced with observationally derived surface forcing.

5. Biases in NCAR CCSM4 and POP2 Simulations

To examine the extent to which the SETA bias may be attributed to ocean model physics and resolution issues, we chose to compare simulations by CCSM4 and its ocean and sea-ice component, POP2. Since both models share the same oceanic component with the same physics and resolution, differences between the simulations should be due to atmospheric forcing only. The POP2 simulation is described in Section 2.6. For this analysis, we took the 21-year period from January 1984 to December 2004 from the last (14th) cycle of the simulation and compared it to the historical CCSM4 simulation for the same time period.

In comparison with the CCSM4 simulation, the POP2 simulation has a weaker SST bias (~1° C) along the equator (Figure 14). This is expected because the POP2 simulation is forced by observationally derived surface forcing and is further constrained by observed surface air-temperatures. As shown by Richter et al. (2012a), replacing erroneous simulated winds along the equator by observed winds alone can substantially reduce the equatorial SST bias. Below the surface, the western equatorial thermocline in POP2 is significantly improved over the CCSM4 simulation and is closer to the NCEP/CFSR reanalysis. The eastern equatorial thermocline, on the other hand, is still too deep and diffuse compared to the reanalysis, resulting in a significant subsurface warm temperature bias (~5°K) that is comparable to or even stronger than that in CCSM4 (Figure 14). Furthermore, between 100m to 200m the temperature bias is even stronger in POP2 than CCSM4, indicating large systematic errors in the eastern equatorial subsurface in POP2, which are likely to be related to the parameterization of vertical mixing or insufficient vertical resolution.

In the SETA, the POP2 simulation produces a prominent SST bias that bears a remarkable similarity to the SST bias pattern in the CCSM4 simulation, albeit with a weaker amplitude that is about half that of the CCSM4 bias. Compared to the CCSM4 simulation, the overshooting problem in the POP2 simulation is improved, but not eliminated. As shown in Figure 16b and 16d, the ABF location, defined by zero near-surface meridional velocity, is at 20°S in POP2, compared to 25°S in CCSM4. Relative to the observations, however, the ABF in POP2 is still shifted southward by 4°. This indicates that at least half of the AC overshooting problem is attributable to systematic errors of POP2, which may be due to the insufficient model resolution.

The CCSM4 and POP2 simulations also share common biases in the upper ocean temperature along the coast of southern Africa. As shown in Figure 16a and 16c, north of the ABF, the thermocline simulated by POP2, similar to that of CCSM4, is too deep and too diffuse compared to NCEP/CFSR reanalysis (Figure 2b), resulting in a significant warm bias off the coast of Angola. Compared to CCSM4, the upper ocean temperature is 2°C colder, consistent with the smaller upstream bias in upper ocean in the equatorial region in POP2. Beneath 100m, however, the temperature bias in CCSM4 actually is smaller than that in POP2 both in the equatorial region and to the north of the front.

South of the ABF, the simulated northward BC is too shallow and too weak in POP2 (Figure 16b) compared to that in NCEP/CFSR reanalysis (Figure 10b), even though it is improved relative to CCSM4. With the observed surface forcing, the POP2 still generates a significant amount of stratified water mass penetrating across the ABF into the Benguela upwelling zone, albeit in less pronounced than in CCSM4, suggesting that the Benguela upwelling simulated by POP2 is too weak compared to observations. This finding indicates that a significant portion of the SETA biases in CCSM4 may stem from systematic errors in POP2, some of which may be attributed to insufficient ocean model resolution that prevents the model from fully resolving the intense upwelling dynamics off the Benguela coast.

To estimate the contribution of the horizontal and vertical heat transport to the local heat budget in CCSM4 and POP2, we compute the upper 100 m heat and volume transport from the western, southern, northern and bottom boundaries of a region in the Benguela upwelling zone indicated by the parallelogram in Figure 17. The results show that the heat (volume) transport into the region by the simulated AC and BC are 186.56±20.03 TW (2.09±0.20 Sv) and 69.79±8.10 TW (0.98±0.12 Sv) in CCSM4, respectively, larger than the corresponding values of 135.10±18.19 TW (1.56±0.21 Sv) and 56.52±7.37 TW (0.80±0.10 Sv) in POP2 at the northern and southern boundaries. This results in a stronger offshore heat (volume) transport of -312.0±19.88 TW (-3.64±0.25 Sv) in CCSM4 than in POP2 (-262.75±25.51 TW (-3.22± 0.35 Sv)), where negative values indicate transport leaving the box. It is interesting to note that even though the BC is stronger in CCSM4 (Figure 16b, 16d), the ABF is located further southward in CCSM4 than in POP2. This is likely due to the bias in the local winds that produces an unrealistically strong wind stress curl in CCSM4 (similar to that shown in Figure 13b), causing the AC to overshoot more severely in CCSM4 than in POP2.

At the bottom boundary (located at 100 m), the directly computed volume transport in POP2 (1.13±0.20 Sv) is 60% stronger than that in CCSM4 (0.81±0.14 Sv), demonstrating the effect of the improvement in the alongshore wind. However, the heat transport from the bottom boundary is much larger in POP2 (71.66±12.60 TW) than in CCSM4 (27.79±4.48 TW). This is because the subsurface temperature is considerably warmer in POP2, resulting in a more severe subsurface warm bias in POP2 than in CCSM4. This stronger subsurface warm bias in POP2 is likely to be related to the stronger subsurface warm bias in the equatorial region in POP2 as shown in Figure 14. A mechanism of how the equatorial subsurface temperature bias can affect the coastal SST bias was proposed and discussed by Xu et al. (2013). It is worth noting that the directly computed vertical volume transports, 0.81±0.14 Sv and 1.13±0.20 Sv, in both CCSM4 and POP2 are higher than the implied values, 0.57 Sv and 0.86 Sv, computed as residual of the horizontal transport. This discrepancy is likely due to sampling and interpolation errors. In general, it is difficult to balance the mass and heat budgets using monthly mean output. In spite of this uncertainty, it is clear from this analysis that horizontal heat transport plays an equally important, if not more important, role as the upwelling process in determining upper ocean heat budget in the Benguela upwelling region. This finding provides further support to the discussion at the end of Section 3.2.

6. Impact of SETA SST Bias

The finding that the strongest tropical Atlantic SST bias is not located within the deep tropics, but confined near and south of the ABF from 15°S to 25°S off the west coast of southern Africa, raises an important question about the impact the SETA SST bias on other regions. Given that the SST bias approaches to 8-9°C in some of the CMIP models, one might expect that the impact of this severe SST warm bias will be significant. Furthermore, one of the most disconcerting features of the SETA warm SST bias is the fact that the region of the severe warm SST bias coincides with the region of the most pronounced SST warming trend over the 20th century (see Figure 2 of Deser et al. 2012). This may undermine the credibility of climate models in detecting, simulating and projecting future climate change in the region.

To further quantify the impact of the SETA SST bias, we performed a set of twin 50-year simulations using the Community Atmosphere Model version 3 (CAM3) at T42 spectral resolution coupled to a slab-ocean-model (SOM). These experiments were designed to isolate SETA SST bias effects from bias influences from other region. In the first simulation (control run), we used an internal heat source Q (also called a Q-flux) in the SOM, which was computed by constraining the modeled SST with the observed SST climatology, so that the SST in SOM resembles closely the observed SST (not shown). In the second simulation (SST-bias run), we set Q to zero over the south tropical Atlantic domain between 30°S-5°S while keeping the globally integrated Q unchanged. This was done as follows: first, the removed Q was integrated over the south tropical Atlantic domain, then divided by the global ocean area from 60°S to 60°N, excluding the south tropical Atlantic domain, and finally the resultant area-average Q (~1 wm^{-2}) was added to the control run Q at each grid point of the global ocean domain. Since the Q-flux represents the missing ocean heat transport in the SOM, one expects large SST biases to appear in the south tropical Atlantic in this simulation due to the altered Q-flux, whereas in all other regions where Q-flux was only changed by a negligibly small amount from the control run, changes in surface temperature can be primarily attributed to the remote influence of the south tropical Atlantic SST biases.

Figure 18 shows the mean surface temperature and precipitation differences between the two simulations (defined as the difference of SST-bias run minus control run averaged over the last 10 simulation years). The large warm SST bias off the coast of southern Africa in the SST-bias simulation bears a remarkable resemblance to the SST bias in the CMIP ensemble shown in Figure 1. Outside of the south tropical Atlantic, cold surface temperature biases are observed over the north tropical Atlantic and the Nordeste region of Brazil, as well as along the equatorial Pacific, while warm surface temperature biases are observed over much of South America and in the off-equatorial regions of the western tropical Pacific (Figure 18a). Consistent with these surface temperature biases, there are wet precipitation biases over the south tropical Atlantic and dry precipitation biases over the north tropical Atlantic and much of South America with the exception of the Nordeste region, indicative of a southward-shift of the Atlantic ITCZ (Figure 18b). Over the tropical Pacific sector, precipitation decreases in a narrow band along the equator and increases north and south of it, particularly over the west-central tropical Pacific. Therefore, with the caveat of potential model dependence, the results do suggest a significant impact of the SETA SST bias on global model simulations of tropical climate. This further underscores the importance and urgency to reduce the SETA SST bias in global climate models.

7. Summary and Discussion

Severe SST biases in the TA are a long-standing problem in CGCMs. Although many of CMIP5 models have improved physics and resolution compared to their predecessor CMIP3 models, TA SST biases remain virtually unchanged. The strongest

SST bias is located at around 16°S near the ABF with a magnitude of more than 6°C in CMIP5 multi-model mean SST. Below the surface along the coast of southern Africa, there is a substantial subsurface warm bias that is most pronounced at about 50m.

On the equator, the SST bias is closely related to the equatorial westerly surface wind bias during boreal spring, which has been attributed to systematic atmospheric model errors in simulating deep convection over the Amazon region (Richter et al. 2012a). South of the equator, the more severe SST biases along the coast of southern Africa have been linked to several mechanisms, including insufficient marine stratus clouds, deficient Benguela upwelling and remote influences from equatorial temperature biases. In this paper, we used CMIP5 datasets combined with reanalyses and observations to test these proposed mechanisms.

Consistent with the stratus cloud hypothesis, we find that CMIP5 models overestimate shortwave radiation in the SETA, resulting in a positive heat flux bias on the order of 20 Wm^{-2}. Although this positive heat flux bias contributes to the warm SST bias in the region, the analysis shows that this contribution is overcompensated for by negative biases in latent heat and longwave fluxes. Therefore, the bias in the net surface heat flux is negative in the region and tends to cool, rather than warm, the surface ocean in the absence of other processes. This result also holds in atmosphere-only GCM simulations forced with observed SST and is not sensitive to the choice of averaging region. A comparison between the atmosphere-only GCM and coupled model simulations reveals a weak stratocumulus-SST feedback in CMIP5 models. Furthermore, there is no correlation between inter-model SST biases and net heat flux biases. Together these findings suggest that the stratus cloud bias is unlikely to be the leading cause of the SST bias in the SETA. It is, however, worth noting that none of the CMIP5 models used in the analysis resolves oceanic eddies. Therefore, it is possible that offshore ocean heat transport is underestimated in these models. In this case, a warm SST bias due to poorly simulated stratus clouds may be overcompensated by an increase in latent heat flux and/or upward longwave heat flux. In the southeast tropical Pacific, the field observations (Colbo and Weller, 2007) and model simulations (Toniazzo et al., 2009) indicate that horizontal heat transport induced by oceanic mesoscale eddies can make a significant contribution to the long-term heat budget of the upper ocean. Whether the eddy-induced ocean heat transport also plays a significant role in the local heat budget in the SETA region requires further study. A full understanding of this issue will require enhanced field observations in the region and eddy-resolving climate model simulations. Future studies are also needed to explore whether there are dynamical processes by which the near-coast SST bias can have an influence on the off-shore biases under the SETA stratocumulus deck.

In terms of coastal upwelling, we found that all CMIP5 models underestimate the Benguela upwelling strength. However, the severity of model upwelling errors is not correlated with the severity of the SETA SST bias, suggesting that upwelling-induced vertical heat advection is not the dominant physical process controlling the SST bias. Instead, the upwelling can indirectly affect the SST bias via horizontal heat advection. This is due to the close dynamical link between the strength of upwelling and that of the BC. The strength of the BC, in turn, determines the position of the ABF, and thus the weak BC in the models is closely linked to their southward displacement of the ABF. Because of the strong temperature gradient near the ABF, errors in the coastal currents can lead to a strong bias in horizontal heat transport that may be as important to the SST biases as the contribution from underrepresented upwelling. A heat budget analysis of CCSM4 and POP2 simulations in the Benguela upwelling region supports this finding.

Regarding the remote influence of equatorial temperature biases, we found a statistically significant correlation between both the surface and subsurface temperature biases in the eastern equatorial region and SETA SST biases in CMIP5 models, suggesting that these equatorial biases do contribute the coastal SST bias. This result supports the finding reported by Toniazzo and Woolnough (2013) that the SST errors along the equatorial Atlantic and Benguela-Angola coast are connected via an oceanic "bridge". However, we also noted that the equatorial temperature biases are generally weaker than the SETA biases and therefore unlikely to be the main error source.

Finally, motivated by the co-location of the SETA SST bias and the ABF, we examined the correlation between ABF latitude and SST biases in CMIP5. The result shows that the two quantities are correlated at the highest level of statistical significance among all the variables that we analyzed. The correlation coefficient between ABF latitude and SST biases is 0.66. Based on this finding, we propose that the inability of CMIP5 models to realistically simulate the ABF is a major cause of the severe SST bias in the SETA.

We further examined whether the erroneous southward displacement of the ABF is caused by surface wind errors in the atmospheric component, or physics and resolution errors in the oceanic component. To this end we compared, for the same period, simulations of CCSM4 and its oceanic component, POP2, run in stand-alone mode and forced with COREII best estimates of surface fluxes. The result shows that about 50% of

CCSM4 biases in the ABF region come from systematic errors of the ocean model. Some of these errors appear to be directly linked to the coarse resolution of POP2 that cannot resolve the ABF and Benguela upwelling. However, it is unlikely that the bias problem can be solved by simply enhancing model resolutions. Kirtman et al. (2012) assessed the impact of ocean model resolution on CCSM climate simulation. Their results revealed little improvement of the warm SST bias in the SETA region when the ocean model horizontal resolution was increased from 1° to 0.1°, while keeping the atmospheric model resolution intact (their Figure 3). Based on the comparison between CCSM4 and POP2 simulations, we estimate that at least 50% of the SETA SST bias may be attributed to the errors in air-sea fluxes, particularly the momentum fluxes (i.e., wind stresses), of the coupled model. CMIP5 models simulate poorly the low level Benguela jet, resulting in a major bias in the simulated alongshore wind stress. The erroneous wind stress distribution in the models causes an excessive negative wind stress curl along the African coast, which is likely to contribute to the overshoot of the AC in CMIP5 models. Furthermore, there are potential positive feedbacks between the intensity of the Benguela jet and the intensity of the coastal upwelling (Nicholson, 2010), which are not well represented by the CMIP models. Future atmospheric model improvements need to focus on dynamical processes governing the Benguela jet. Improved observations are also needed to provide a more detailed and accurate characterization of the low level jet and the alongshore winds, allowing for better model validation.

Finally, we assessed the impact of the SETA SST bias on global climate simulations by conducting a set of twin CAM3-SOM simulations. The results indicate that even though the SST bias is confined in a relative small region in the southeast

Atlantic, its impact goes far beyond the southeast Atlantic. In addition to affecting the Atlantic ITCZ and rainfall pattern over South America, the SETA SST bias exerts a remote influence on rainfall pattern over the western tropical Pacific and exacerbate the double ITCZ problem in that region. Therefore, it is likely that the severe SST bias over the relatively small southeast Atlantic region in current generation climate models can deteriorate simulations of the large-scale atmospheric circulation. As such, understanding causes of the biases and improving climate models' representations of physical processes contributing to this bias should be considered near-term high priority research areas in the climate research community.

Acknowledgements

We are grateful to Paquita Zuidema and C. Roberto Mechoso for their insightful comments, which improved this paper significantly. This research is supported by the U.S. National Science Foundation Grants, OCE-1334707 and AGS-1067937, and Department of Energy Grant DE-SC0006824, as well as National Oceanic and Atmospheric Administration Grant NA11OAR4310154. PC acknowledges the support from the National Science Foundation of China (41028005, 40921004 and 40930844).

References

Bretherton, C. S., T. Uttal, C. W. Fairall, S. E. Yuter, R. A. Weller, D. Baumgardner, K. Comstock, and R. Wood, 2004: The EPIC 2001 stratocumulus study. Bull. Amer. Meteor. Soc., 85, 967–977.

Carton, J. A., and B. S. Giese, 2008: A reanalysis of ocean climate using Simple Ocean Data Assimilation (SODA). Monthly Weather Review, 136, 2999-3017.

Carton, J. A., B. S. Giese, and S. A. Grodsky, 2005: Sea level rise and the warming of the oceans in the Simple Ocean Data Assimilation (SODA) ocean reanalysis. Journal of Geophysical Research, 110.

Chang, C.-Y., J. A. Carton, S. A. Grodsky, and S. Nigam, 2007: Seasonal climate of the tropical Atlantic sector in the NCAR community climate system model 3: Error structure and probable causes of errors. Journal of Climate, 20, 1053-1070.

Chassignet, E. P., and Coauthors, 2007: The HYCOM (HYbrid Coordinate Ocean Model) data assimilative system. Journal of Marine Systems, 65, 60-83.

Colberg, F., and C. J. C. Reason, 2006: A model study of the Angola Benguela Frontal Zone: Sensitivity to atmospheric forcing. Geophysical Research Letters, 33.

Colbo, K., and R. Weller, 2007: The variability and heat budget of the upper ocean under the Chile-Peru stratus. J. Mar. Res., 65, 607–637.

Dai, A. C., 2006: Precipitation characteristics in eighteen coupled climate models. Journal of Climate, 9, 4605-4630.

Davey, M. K., and Coauthors, 2002: STOIC: a study of coupled model climatology and variability in tropical ocean regions. Climate Dynamics, 18, 403-420.

Deser, C., A. S. Phillips, and M. A. Alexander (2010), Twentieth century tropical sea surface temperature trends revisited, Geophys Res Lett, 37, DOI 10.1029/2010GL043321.

de Szoeke, S. P., and S.-P. Xie, 2008: The tropical east- ern Pacific seasonal cycle: Assessment of errors and mechanisms in IPCC AR4 coupled ocean–general circulation models. *J. Climate*, 21, 2573–2590.

de Szoeke, S. P., C. W. Fairall, D. E. Wolfe, L. Bariteau, and P. Zuidema, 2010: Surface flux observations on the southeastern tropical Pacific Ocean and attribution of SST errors in coupled ocean–atmosphere models. *J. Climate*, 23, 4152–4174.

de Szoeke, S. P., S. Yuter, D. Mechem, C.W. Fairall, C.D. Burleyson, and P. Zuidema, 2012: Observations of stratocumulus clouds and their effects on the Eastern Pacific surface heat budget along 20°S, Journal of Climate, 25, 8542-8567, DOI: 10.1175/JCLI-D-11-00618.1

DeWitt, D. G., 2005: Diagnosis of the tropical Atlantic near-equatorial SST bias in a directly coupled atmosphere-ocean general circulation model. Geophysical Research Letters, 32.

Doi, T., G. A. Vecchi, A. J. Rosati, and T. L. Delworth, 2012: Biases in the Atlantic ITCZ in seasonal–interannual variations for a coarse- and a high-resolution coupled climate model. Journal of Climate, 25, 5494-5511.

Fennel, W., T. Tucker, M. Schimdt and V. Mohrholz, 2012: Response of the Benguela upwelling systems to spatial variations in the wind stress. Continental Shelf Research, 45, 65-77.

Garreaud, R. D., and R. C. Muñoz, 2005: The low-level jet off the west coast of subtropical South America: Structure and variability. *Mon. Wea. Rev.*, 133, 2246–2261.

Grodsky, S. A., J. A. Carton, S. Nigam, and Y. M. Okumura, 2012: Tropical Atlantic biases in CCSM4. Journal of Climate, 25, 3684-3701.

Hu, Z.-Z., B. Huang, and K. Pegion, 2008: Low cloud errors over the southeastern Atlantic in the NCEP CFS and their association with lower-tropospheric stability and air-sea interaction. Journal of Geophysical Research, 113.

Huang, B., 2004: Remotely forced variability in the tropical Atlantic Ocean. Climate Dynamics, 23.

Huang, B., Z.-Z. Hu, and B. Jha, 2007: Evolution of model systematic errors in the Tropical Atlantic Basin from coupled climate hindcasts. Climate Dynamics, 28, 661-682.

Kirtman, B.P. and Coauthors, 2012: Impact of ocean model resolution on CCSM climate simulations, Climate Dynamics, 39, 1303-1328, DOI 10.1007/s00382-012-1500-3.

Large, W. G., and S. G. Yeager, 2004: Diurnal to decadal global forcing for ocean and seaice models: the data sets and climatologies. Technical Report, 105 pp.

Large, W. G., and G. Danabasoglu, 2006: Attribution and impacts of upper-ocean biases in CCSM3. Journal of Climate, 19, 2325-2346.

Large, W. G., and S. G. Yeager, 2008: The global climatology of an interannually varying air–sea flux data set. Climate Dynamics, 33, 341-364.

Lass, H. U., M. Schmidt, V. Mohrholz, and G. Nausch, 2000: Hydrographic and current measurements in the area of the Angola–Benguela front. Journal of Physical Oceanography, 30, 2589–2609.

Ma, C.-C., C. R. Mechoso, A. W. Robertson, and A. Arakawa, 1996: Peruvian stratus clouds and the tropical pacific circulation: a coupled ocean-atmosphere GCM study. Journal of Climate, 9, 1635-1645.

Mechoso, C. R., and Coauthors, 1995: The seasonal cycle over the tropical Pacific in general circulation models. Mon. Wea. Rev., 123, 2825–2838.

Mechoso, C. R., and R. Wood, 2010: An abbreviated history of VOCALS. CLIVAR Exchanges, 53, International CLIVAR Project Office, Southampton, United Kingdom, 3–5.

Mechoso and co-authors, 2014: Ocean-cloud-atmopshere-land interaction in the southeastern Pacific: the VOCALS program, Bull. Amer. Meteor. Soc., doi: http://dx.doi.org/10.1175/BAMS-D-11-00246.1

Meehl, G. A., and Coauthors, 2007: The WCRP CMIP3 multimodel dataset: a new era in climate change research, Bulletin of the American Meteorological Society, 88, 1383-1394.

R. C. Muñoz and Garreaud, R. D., 2005: Dynamics of the low-level jet off the west coast of subtropical South America, . *Mon. Wea. Rev.*, 133, 3661–3677.

Nicholson, S.E., 2010: A low-level jet along the Benguela coast, an integral part of the Benguela current ecosystem, Climate Change, 99, 613-624, DOI 10.1007/s10584-009-9678-z.

Nigam, S., 1997: The annual warm to cold phase transition in the eastern equatorial Pacific: diagnosis of the role of stratus cloud-top cooling. Journal of Climate, 10, 2447-2467.

Patricola, C. M., M. Li, Z. Xu, P. Chang, R. Saravanan, and J.-S. Hsieh, 2011: An investigation of tropical Atlantic bias in a high-resolution coupled regional climate model. Climate Dynamics, 39, 2443-2463.

Penven, P., V. Echevin, J. Pasapera, F. Colas, and J. Tam, 2005: Average circulation, seasonal cycle, and mesoscale dynamics of the Peru current system: a modeling approach. Journal of Geophysical Research-Oceans, 110, doi:10.1029/2005JC002945 .

Peterson, R. G., and L. Stramma, 1991: Upper-level circulation in the south Atlantic ocean. Progress in Oceanography, 26, 1-73.

Reynolds, R. W., T. M. Smith, C. Liu, D. B. Chelton, K. S. Casey, and M. G. Schlax, 2007: Daily high-resolution-blended analyses for sea surface temperature. Journal of Climate, 20, 5473-5496.

Richter, I., C.R. Mechoso, and A.W. Robertson, 2008: What Determines the Position and Intensity of the South Atlantic Anticyclone in Austral Winter?—An AGCM Study. J. Climate, 21, 214–229.

Richter, I., and S.-P. Xie, 2008: On the origin of equatorial Atlantic biases in coupled general circulation models. Climate Dynamics, 31, 587-598.

Richter I., Xie S-P, Wittenberg AT, Masumoto Y, 2012a: Tropical Atlantic biases and their relation to surface wind stress and terrestrial precipitation. Clim Dyn: 38: 985–1001, doi:10.1007/s00382-011-1038-9.

Richter I, Xie S-P, Behera SK, Doi T, Masumoto Y, 2012b: Equatorial Atlantic variability and its relation to mean state biases in CMIP5. Clim Dyn, doi: 10.1007/s00382-012-1624-5

Saha, S., and Coauthors, 2010: The NCEP Climate Forecast System Reanalysis. Bulletin of the American Meteorological Society, 91, 1015-1057.

Seo, H., M. Jochum, R. Murtugudde, and A. J. Miller, 2006: Effect of ocean mesoscale variability on the mean state of tropical Atlantic climate. Geophysical Research Letters, 33.

Taylor, K. E., R. J. Stouffer, and G. A. Meehl, 2012: An overview of CMIP5 and the experiment design. Bulletin of the American Meteorological Society, 93, 485-498.

Toniazzo, T., C. R. Mechoso, L. Shaffrey, and J. M. Slingo, 2009: Upper-ocean heat budget and ocean eddy transport in the south-east Pacific in a high resolution coupled model. Climate Dyn., 35, 1309–1329, doi:10.1007/s00382-009-0703-8.

Wacongne, S., and B. Piton, 1992: The near-surface circulation in the northeastern corner of the South Atlantic ocean. Deep Sea Research Part A. Oceanographic Research Papers, 39, 1273-1298.

Wahl, S., M. Latif, W. Park, and N. Keenlyside, 2009: On the tropical Atlantic SST warm bias in the Kiel Climate Model. Climate Dynamics, 36, 891-906.

Xu, Z., Li, M. and Chang, P, 2013: Oceanic origins of biases in southeast tropical Atlantic. Submitted to Climate Dynamics.

Yamagata, T., and S. Iizuka, 1995: Simulation of the tropical thermal domes in the Atlantic-a Seasonal Cycle. Journal of Physical Oceanography, 25, 2129-2140.

Yu, J. Y., and C. R. Mechoso, 1999: A discussion on the errors in the surface heat fluxes simulated by a coupled GCM. Journal of Climate, 12, 416-426.

Yu, L. S., R. A. Weller, and B. M. Sun, 2004: Mean and variability of the WHOI daily latent and sensible heat fluxes at in situ flux measurement sites in the Atlantic Ocean. Journal of Climate, 17, 2096-2118.

Table 1. List of CMIP5 and AMIP models used in this study and their corresponding institutes and experiment names. Asterisks indicate the AMIP ensemble members and apostrophes indicate the CMIP5 ensemble members. The corresponding “historical” models for HadGEM2-A and CanAM4 are HadGEM2-ES and CanESM2, respectively.

Table 2. Frequency of surface forcing input for the POP2 simulation.

Modeling Center (or Group)	Institute ID	Model Name
Commonwealth Scientific and Industrial Research Organization (CSIRO) and Bureau of Meteorology (BOM), Australia	CSIRO-BOM	ACCESS1.0*' ACCESS1.3*'
Beijing Climate Center, China Meteorological Administration	BCC	BCC-CSM1.1*' BCC-CSM1.1(m)*'
College of Global Change and Earth System Science, Beijing Normal University	GCESS	BNU-ESM*
Canadian Centre for Climate Modelling and Analysis	CCCMA	CanAM4* CanESM2'
National Center for Atmospheric Research	NCAR	CCSM4*'
Community Earth System Model Contributors	NSF-DOE-NCAR	CESM1(BGC)' CESM1(CAM5)*' CESM1(FASTCHEM)' CESM1(WACCM)"
NOAA Geophysical Fluid Dynamics Laboratory	NOAA GFDL	GFDL-CM3*" GFDL-ESM2M'
NASA Goddard Institute for Space Studies	NASA GISS	GISS-E2-H' GISS-E2-H-CC'

		GISS-E2-R*' GISS-E2-R-CC'
Met Office Hadley Centre (additional HadGEM2-ES realizations contributed by Instituto Nacional de Pesquisas Espaciais)	MOHC (additional realizations by INPE)	HadCM3' HadGEM2-A* HadGEM2-CC' HadGEM2-ES'
Institute for Numerical Mathematics	INM	INM-CM4*'
Japan Agency for Marine-Earth Science and Technology, Atmosphere and Ocean Research Institute (The University of Tokyo), and National Institute for Environmental Studies	MIROC	MIROC-ESM' MIROC-ESM-CHEM'
Atmosphere and Ocean Research Institute (The University of Tokyo), National Institute for Environmental Studies, and Japan Agency for Marine-Earth Science and Technology	MIROC	MIROC4h' MIROC5*'
Max-Planck-Institut für Meteorologie (Max Planck Institute for Meteorology)	MPI-M	MPI-ESM-MR*' MPI-ESM-LR*' MPI-ESM-P'
Meteorological Research Institute	MRI	MRI-CGCM3*'
Norwegian Climate Centre	NCC	NorESM1-M*' NorESM1-ME'

Table 1. List of CMIP5 and AMIP models used in this study and their corresponding institutes and experiment names. Asterisks indicate the AMIP ensemble members and apostrophes indicate the CMIP5 ensemble members. The corresponding “historical” models for HadGEM2-A and CanAM4 are HadGEM2-ES and CanESM2, respectively.

Surface forcing	Temporal frequency
Surface Wind	6 hourly
Air temperature	6 hourly
Air humidity	6 hourly
Sea level pressure	6 hourly
Precipitation	Monthly
Short-wave radiation	6 hourly
Long-wave radiation	6 hourly

Table 2. Frequency of surface forcing input for the POP2 simulation.

Figure 1 Multi-model mean SST biases (°C) in (a) CMIP5 and (b) CMIP3, compared to Reynolds SST averaged over the same time period. The difference between CMIP3 and CMIP5 SST biases is shown in (c) and SST zonal gradient averaged between 2°S and 2°N is shown in (d). In (d), the green solid line represents the multi-model mean of CMIP5, the red line represents CMIP3 and the black line represents Reynolds SST. The multi-model standard deviation (STD) is indicated by shading in corresponding colors. The box in (a) indicates the SETA region (5-20°E, 30-10°S) where most of the analysis is performed.

Figure 2 Subsurface temperature profiles (°C) along the African coast in the east Atlantic basin in (a) CMIP5, (b) NCEP-CFSR, and (c) the difference between CMIP5 and CFSR. The alongshore section is defined as the zonal average over a one-degree wide band along the coastline.

Figure 3 21 year (1984-2004) averaged shortwave radiation (W m^{-2}) in (a) OAFlux and (c) CMIP5, and longwave radiation in (b) OAFlux and (d) CMIP5. The black box in (a) indicates the maximum stratocumulus cloud deck region (5°W -10°E, 25-10°S).

Figure 4 Each component of surface heat flux and the net heat flux (W m^{-2}) averaged over the SETA region (5°E to 20°E, 30°S to 10°S) (a) and the main stratocumulus deck region (5°W to 10°E, 25°S to 10°S) (b), respectively, in CMIP5 (red), AMIP(yellow), OAFlux (green) and the difference (blue). The error bars represent the multi-model standard deviations in CMIP5 and AMIP.

Figure 5 (a) shortwave radiation, (b) longwave radiation, (c) sensible heat flux and (d) latent heat flux biases (W m^{-2}) in CMIP5 in the tropical Atlantic. All the biases are averaged from 1984 to 2004 and relative to OAFlux.

Figure 6 Surface net heat flux (W m^{-2}) bias in tropical Atlantic.

Figure 7 Scatter plots of SST bias (°C) averaged from 5°E to 20°E, 30°S to 10°S and (a) heat flux bias (W m^{-2}) in the same region, (b) vertical mass transport (kg s^{-1}) averaged from 10°S to 30°S within 3° along the coast, (c) the equatorial subsurface temperature bias (°C; averaged over 5°W to 10°E, 2°S to 2°N, and 20m-100m), (d) the upstream SST bias (°C; averaged over 0°-15°E, 10°S to 0°). Each symbol represents one model and the red dashed line is the linear fit. Red (black) font for R^2 in this and other following scatter plots indicates that the correlation coefficient passes (does not pass) the 90% significance level.

Figure 8 Scatter plots of alongshore wind stress (N m^{-2}) and (a) vertical mass transport (kg s^{-1}) and (b) SST bias (°C). Averaging areas are 5°E to 20°E, 30°S to 10°S for SST, African coast to 5° off-shore, 0°S to 30°S for wind stress, and vertical mass transport is African coast to 3° off-shore, 10°S to 30°S for vertical mass transport.

Figure 9 SST (°C; shading) and surface currents (cm s^{-1}) in the SETA for (a) CFSR, (b) CMIP5, and SST bias of CMIP5 (shading; bias relative to Reynolds SST) and CMIP5 surface currents (vectors).

Figure 10 Alongshore subsurface meridional current profile (cm s^{-1}) in (a) CMIP5 and (b) CFSR. The averaging region for meridional velocity is the same as that for temperature in Figure 4.

Figure 11 Scatter plot of ABF latitude in CMIP5 and SST bias (°C). Each symbol represents the front location and its corresponding SST bias in one CMIP5 model. The front location is defined as the latitude where zonally averaged meridional velocity within 3 degree along the coast equals to zero.

Figure 12 Surface wind stress (N m^{-2}; vectors) and its magnitude (shading) in (a) CMIP5, (b) COREII, and (c) the difference between CMIP5 and COREII. The wind stress is 11 year mean from 1997 to 2007. In (c), the shading is the difference between the magnitude of (a) and (b), not the magnitude of vectors in (c).

Figure 13 Surface wind stress curl (N m^{-3}) in (a) COREII and (b) CMIP5 averaged from 1997 to 2007.

Figure 14 Subsurface temperature bias relative to NCEP/CFSR (°C; shading) and zonal ocean currents (cm s^{-1}; contours) profiles in (a) POP2 and (b) CCSM4 averaged from 2°S to 2°N and from 1984 to 2004. The solid contours represent positive (eastward) velocity and dashed contours represent negative (westward) velocity.

Figure 15 SST bias (°C; shading) and surface currents (cm s^{-1}; vectors) in (a) CCSM4 and (b) POP.

Figure 16 Subsurface temperature biases (°C) in (a) POP and (c) CCSM, relative to CFSR, and meridional current (cm s^{-1}) in (b) POP and (d) CCSM4.

Figure 17 Upper 100m oceanic advection and convection heat transport and volume transport in the BC region in (a) CCSM4 and (b) POP2.

Figure 18 Surface temperature difference (a, in °C) and precipitation difference (b, in mmd^{-1}) between SST-bias run and control run. The regions marked by “+” indicate that the difference is significant at 95% level based a student T-test.

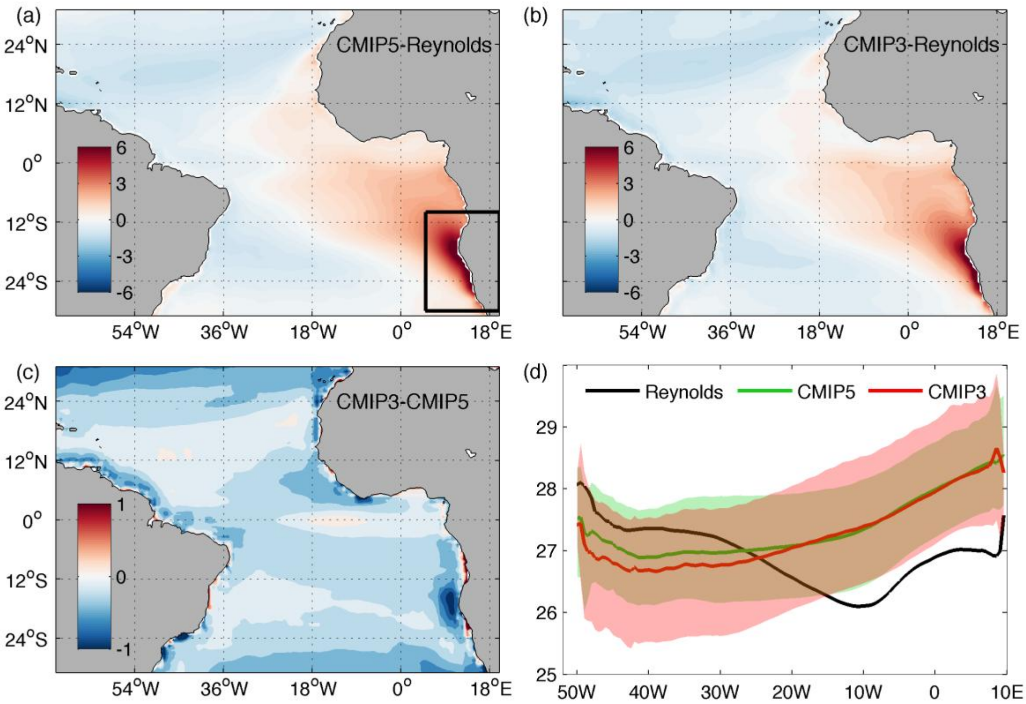

Figure 1 Multi-model mean SST biases (°C) in (a) CMIP5 and (b) CMIP3, compared to Reynolds SST averaged over the same time period. The difference between CMIP3 and CMIP5 SST biases is shown in (c) and SST zonal gradient averaged between 2°S and 2°N is shown in (d). In (d), the green solid line represents the multi-model mean of CMIP5, the red line represents CMIP3 and the black line represents Reynolds SST. The multi-model standard deviation (STD) is indicated by shading in corresponding colors. The box in (a) indicates the SETA region (5-20°E, 30-10°S) where most of the analysis is performed.

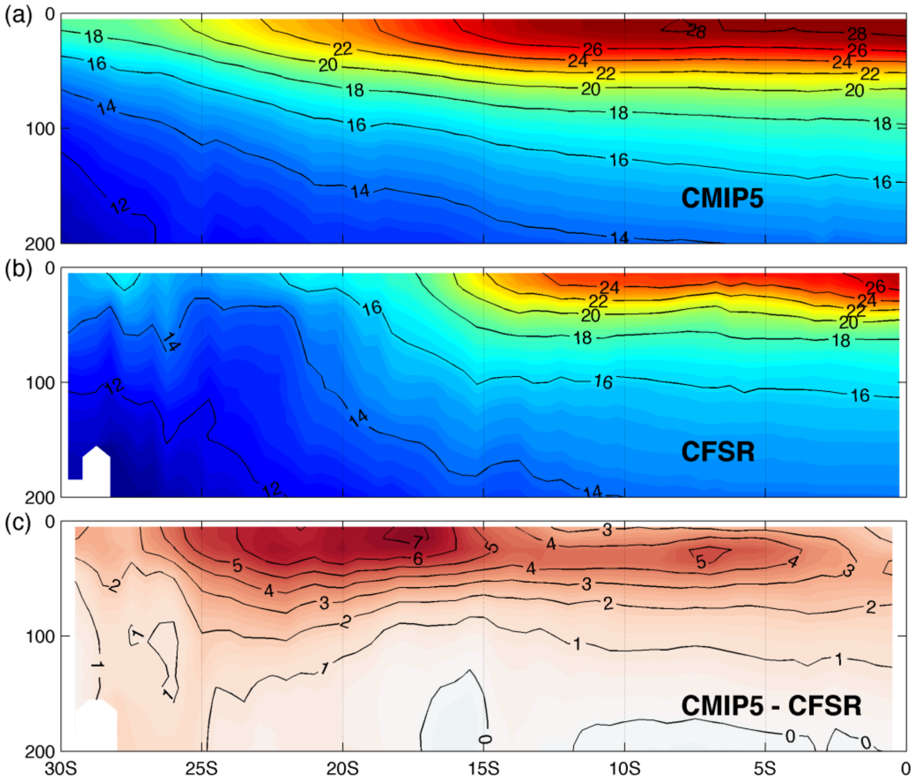

Figure 2 Subsurface temperature profiles (°C) along the African coast in the east Atlantic basin in (a) CMIP5, (b) NCEP-CFSR, and (c) the difference between CMIP5 and CFSR. The alongshore section is defined as the zonal average over a one-degree wide band along the coastline.

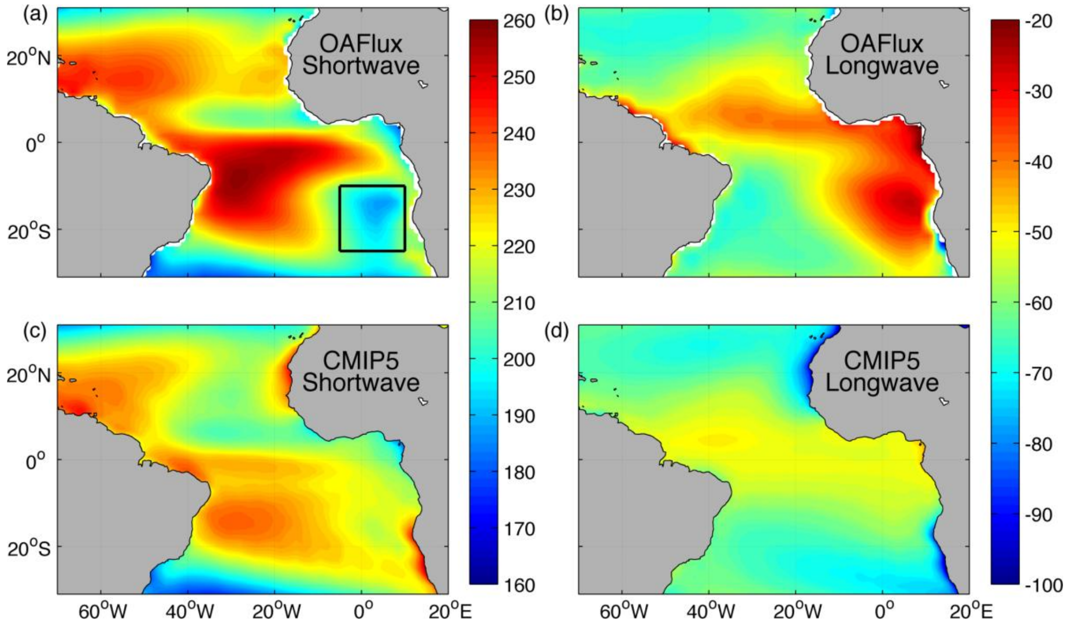

Figure 3 21 year (1984-2004) averaged shortwave radiation (W m^{-2}) in (a) OAFlux and (c) CMIP5, and longwave radiation in (b) OAFlux and (d) CMIP5. The black box in (a) indicates the maximum stratocumulus cloud deck region (5°W -10°E, 25-10°S).

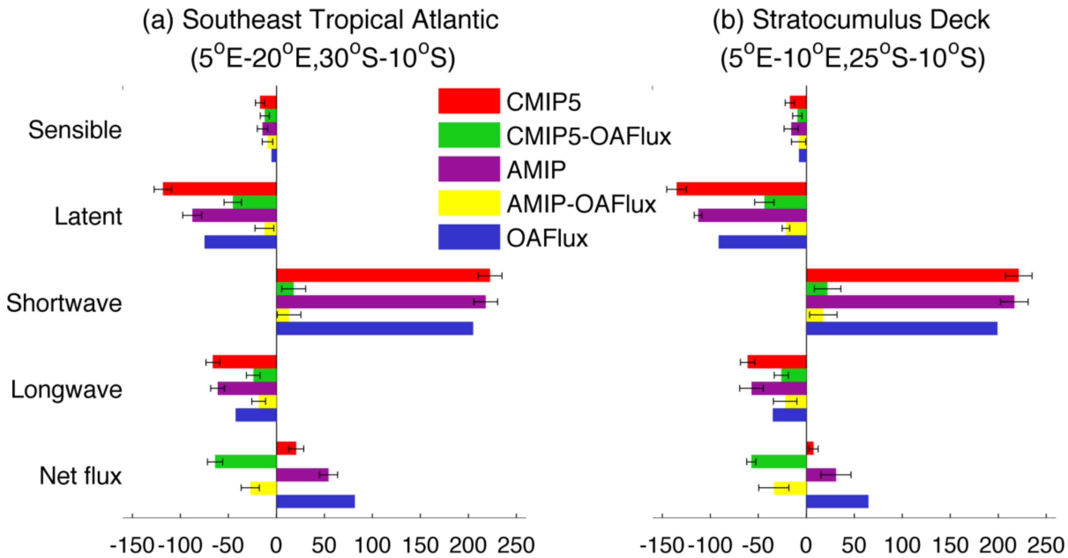

Figure 4 Each component of surface heat flux and the net heat flux (W m^{-2}) averaged over the SETA region (5°E to 20°E, 30°S to 10°S) (a) and the main stratocumulus deck region (5°W to 10°E, 25°S to 10°S) (b), respectively, in CMIP5 (red), AMIP(yellow), OAFlux (green) and the difference (blue). The error bars represent the multi-model standard deviations in CMIP5 and AMIP.

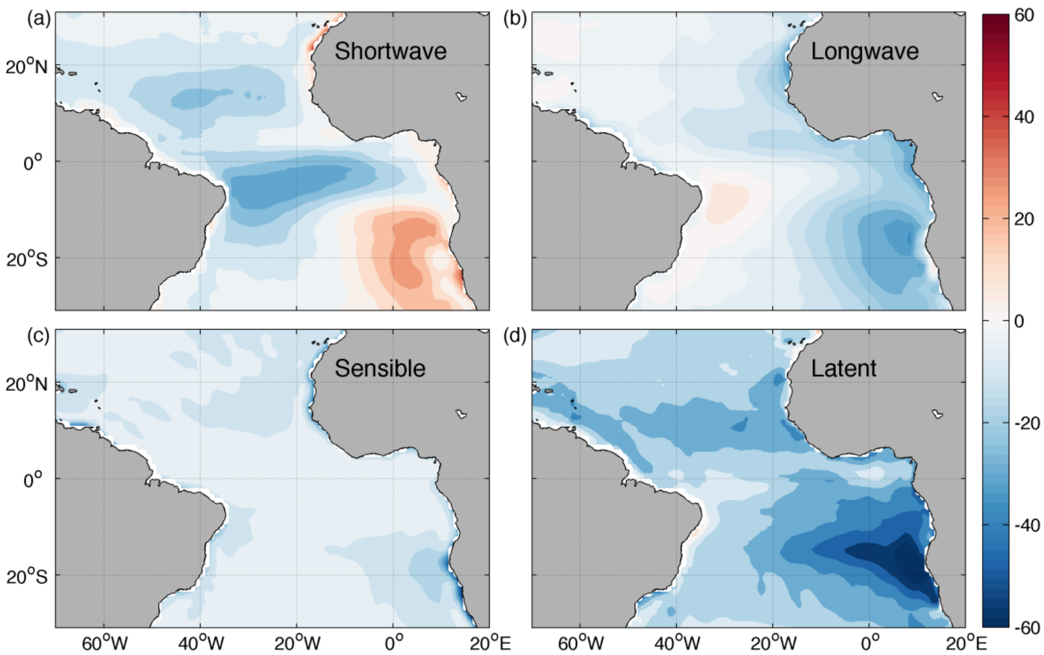

Figure 5 (a) shortwave radiation, (b) longwave radiation, (c) sensible heat flux and (d) latent heat flux biases (W m^{-2}) in CMIP5 in the tropical Atlantic. All the biases are averaged from 1984 to 2004 and relative to OAFlux.

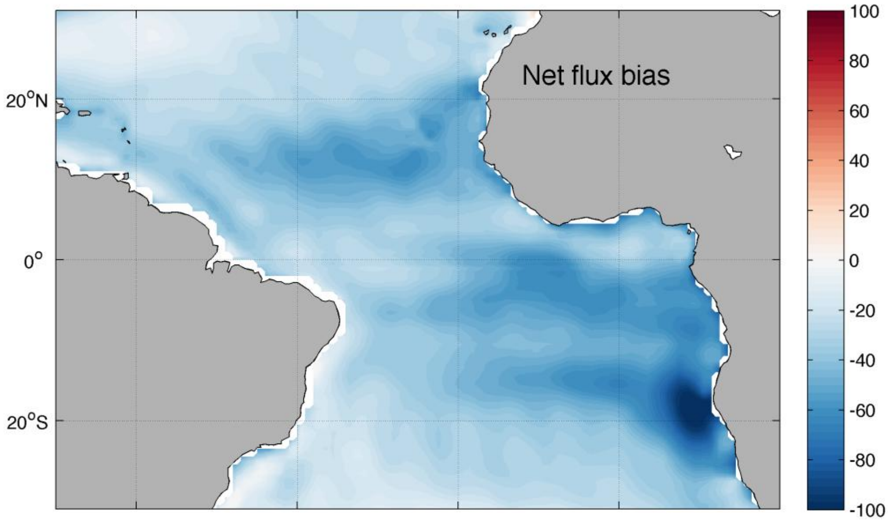

Figure 6 Surface net heat flux (W m^{-2}) bias in tropical Atlantic.

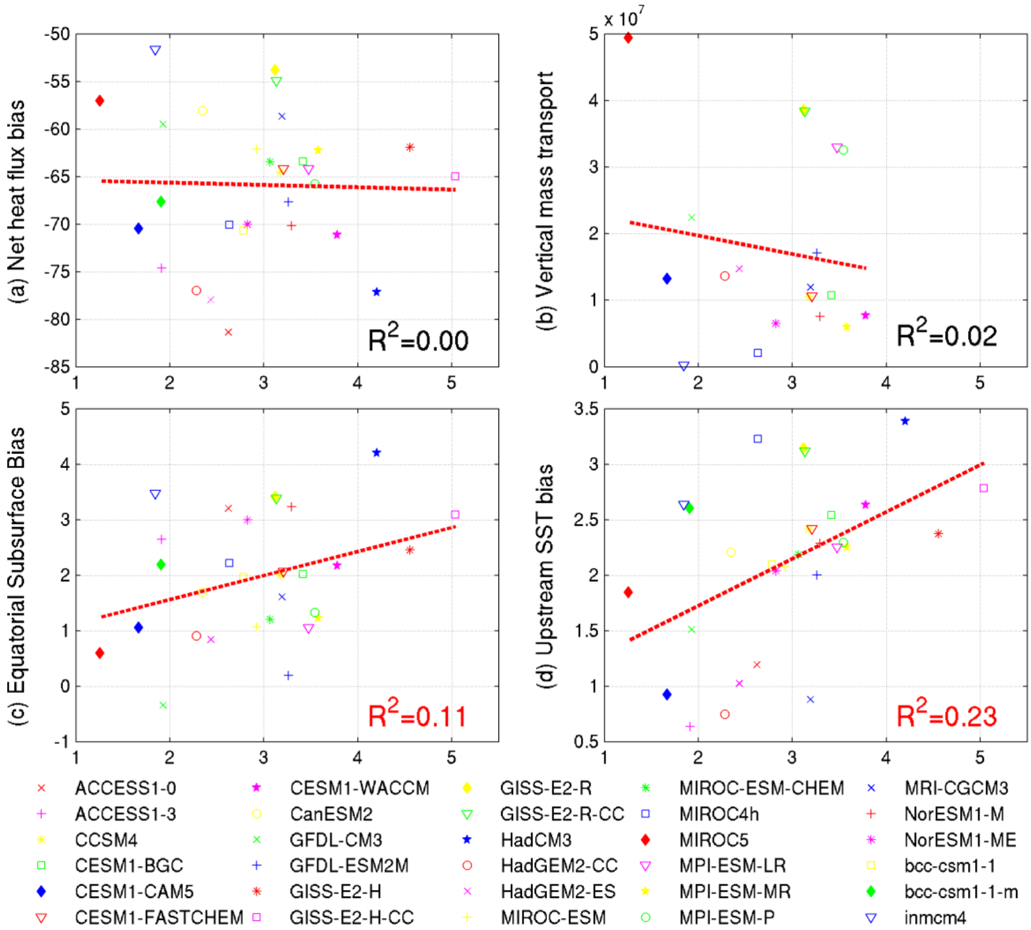

Figure 7 Scatter plots of SST bias (°C) averaged from 5°E to 20°E, 30°S to 10°S and (a) heat flux bias (W m^{-2}) in the same region, (b) vertical mass transport (kg s^{-1}) averaged from 10°S to 30°S within 3° along the coast, (c) the equatorial subsurface temperature bias (°C; averaged over 5°W to 10°E, 2°S to 2°N, and 20m-100m), (d) the upstream SST bias (°C; averaged over 0°-15°E, 10°S to 0°). Each symbol represents one model and the red dashed line is the linear fit. Red (black) font for R^2 in this and other following scatter plots indicates that the correlation coefficient passes (does not pass) the 90% significance level.

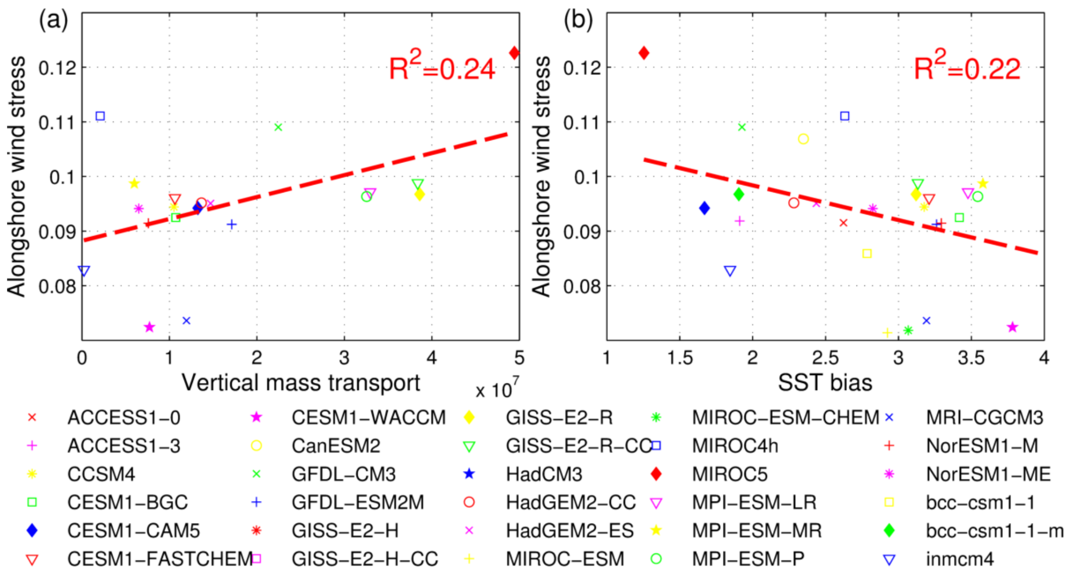

Figure 8 Scatter plots of alongshore wind stress (N m^{-2}) and (a) vertical mass transport (kg s^{-1}) and (b) SST bias (°C). Averaging areas are 5°E to 20°E, 30°S to 10°S for SST, African coast to 5° off-shore, 0°S to 30°S for wind stress, and vertical mass transport is African coast to 3° off-shore, 10°S to 30°S for vertical mass transport.

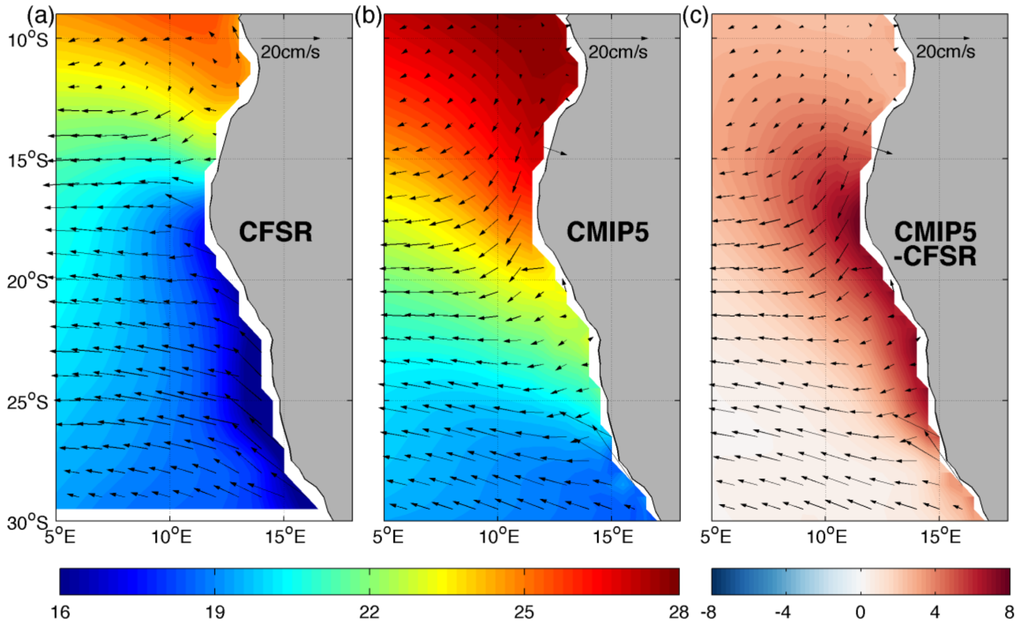

Figure 9 SST (°C; shading) and surface currents (cm s^{-1}; vectors) in the SETA for (a) CFSR, (b) CMIP5, and SST bias of CMIP5 (shading; bias relative to Reynolds SST) and CMIP5 surface currents (vectors).

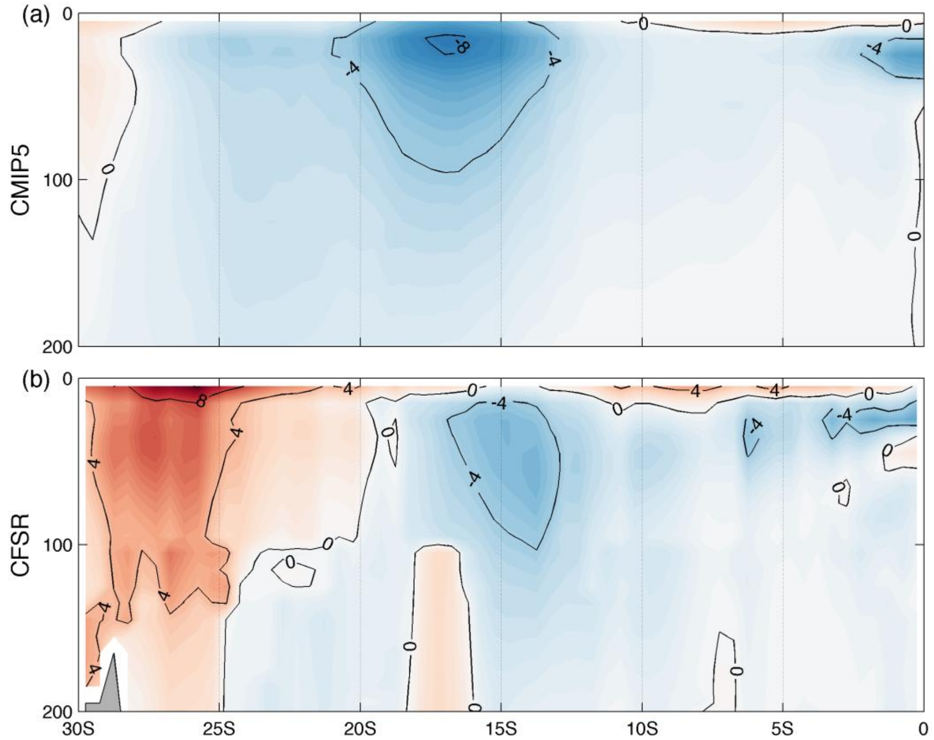

Figure 10 Alongshore subsurface meridional current profile (cm s^{-1}) in (a) CMIP5 and (b) CFSR. The averaging region for meridional velocity is the same as that for temperature in Figure 4.

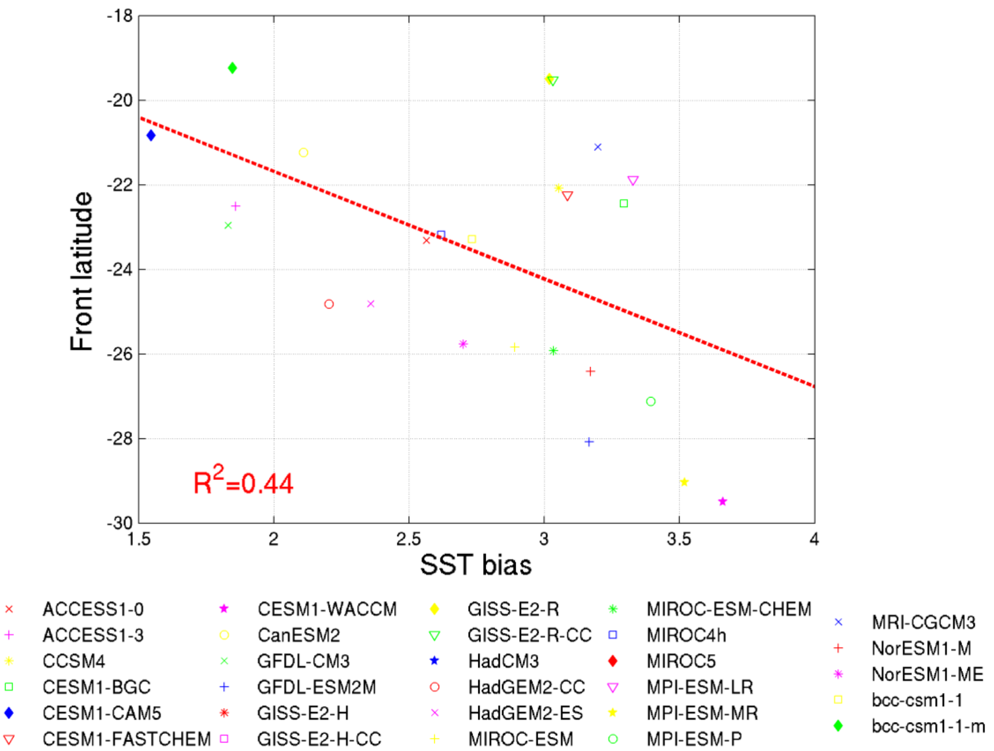

Figure 11 Scatter plot of ABF latitude in CMIP5 and SST bias (°C). Each symbol represents the front location and its corresponding SST bias in one CMIP5 model. The front location is defined as the latitude where zonally averaged meridional velocity within 3 degree along the coast equals to zero.

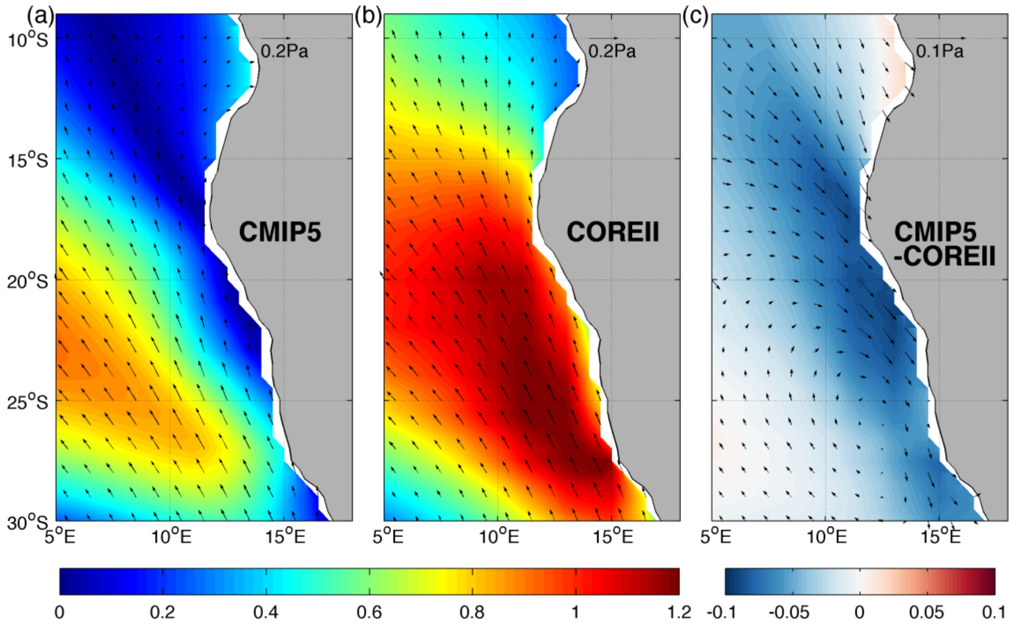

Figure 12 Surface wind stress (N m^{-2}; vectors) and its magnitude (shading) in (a) CMIP5, (b) COREII, and (c) the difference between CMIP5 and COREII. The wind stress is 11-year mean from 1997 to 2007. In (c), the shading is the difference between the magnitude of (a) and (b), not the magnitude of vectors in (c).

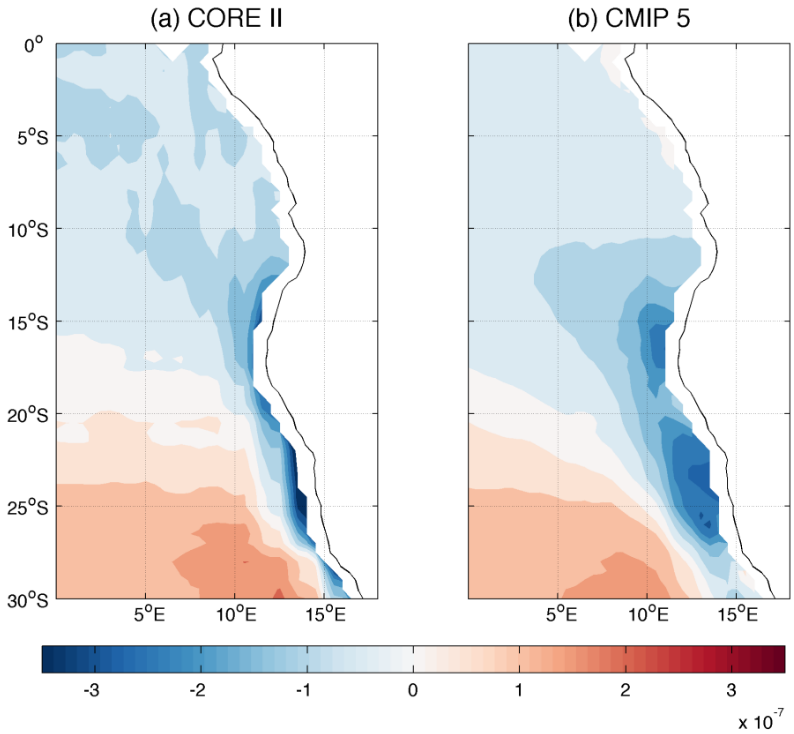

Figure 13 Surface wind stress curl (N m^{-3}) in (a) COREII and (b) CMIP5 averaged from 1997 to 2007.

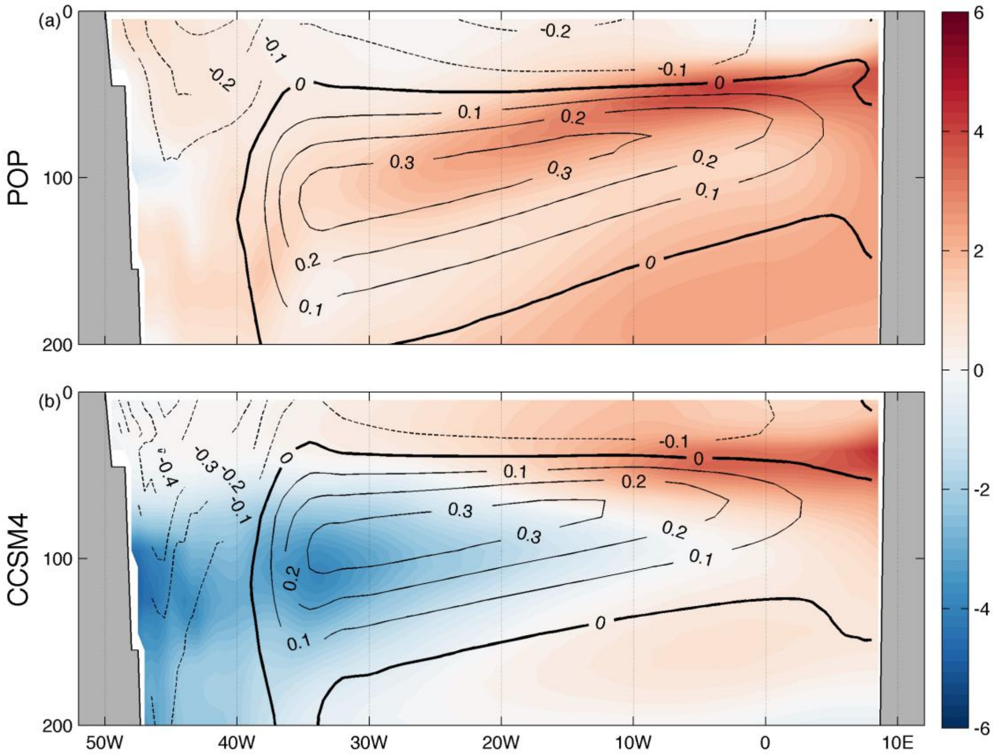

Figure 14 Subsurface temperature bias relative to NCEP/CFSR (°C; shading) and zonal ocean currents (cm s^{-1}; contours) profiles in (a) POP2 and (b) CCSM4 averaged from 2°S to 2°N and from 1984 to 2004. The solid contours represent positive (eastward) velocity and dashed contours represent negative (westward) velocity.

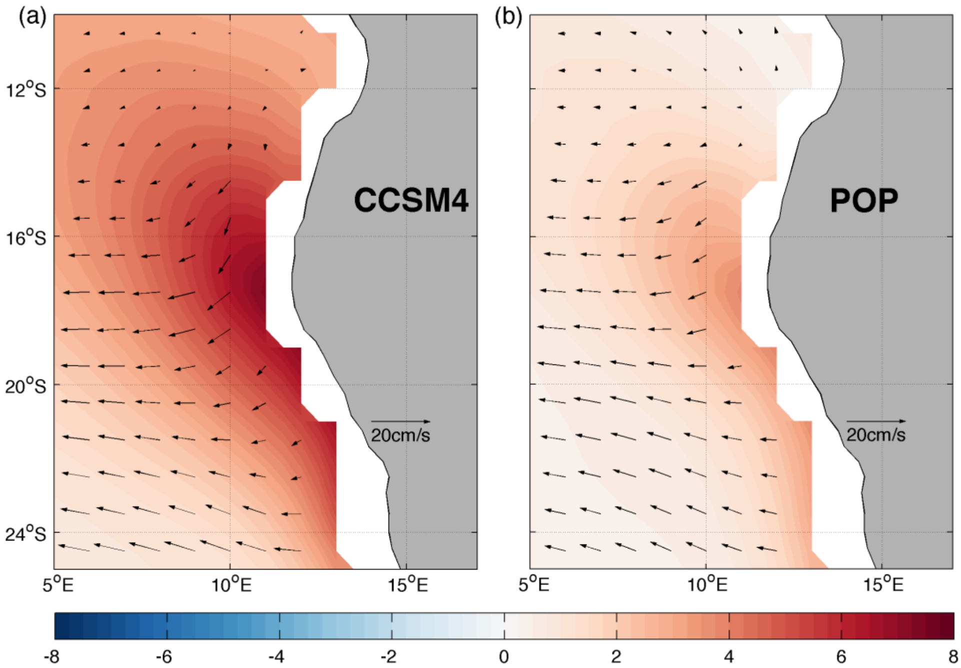

Figure 15 SST bias (°C; shading) and surface currents (cm s^{-1}; vectors) in (a) CCSM4 and (b) POP.

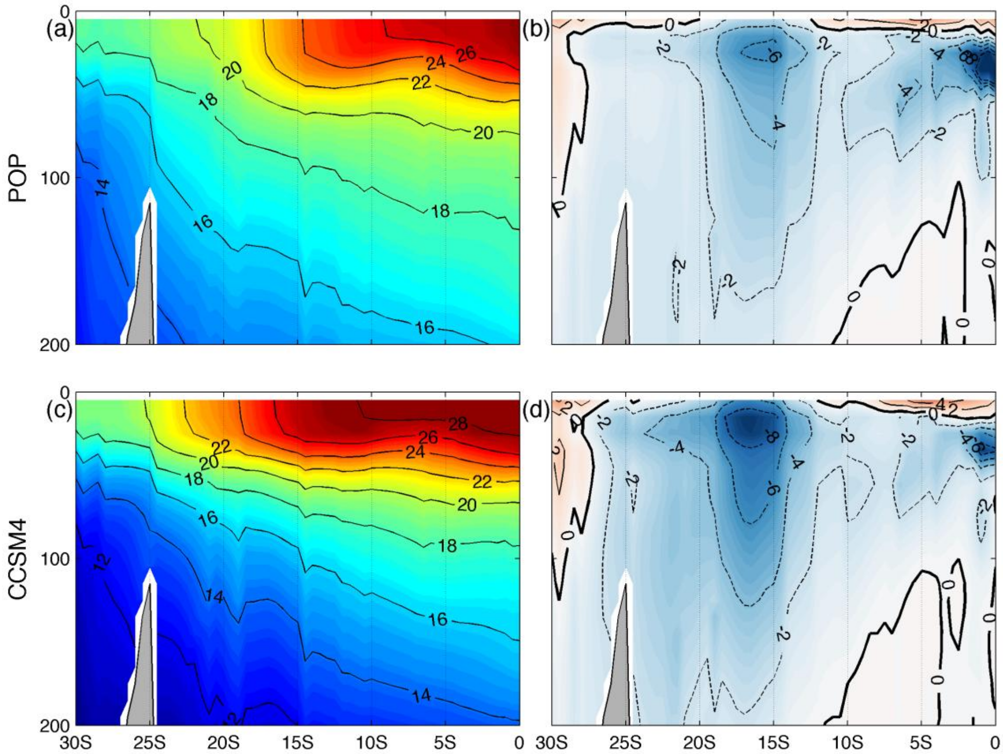

Figure 16 Subsurface temperature biases (°C) in (a) POP and (c) CCSM, relative to CFSR, and meridional current (cm s^{-1}) in (b) POP and (d) CCSM4.

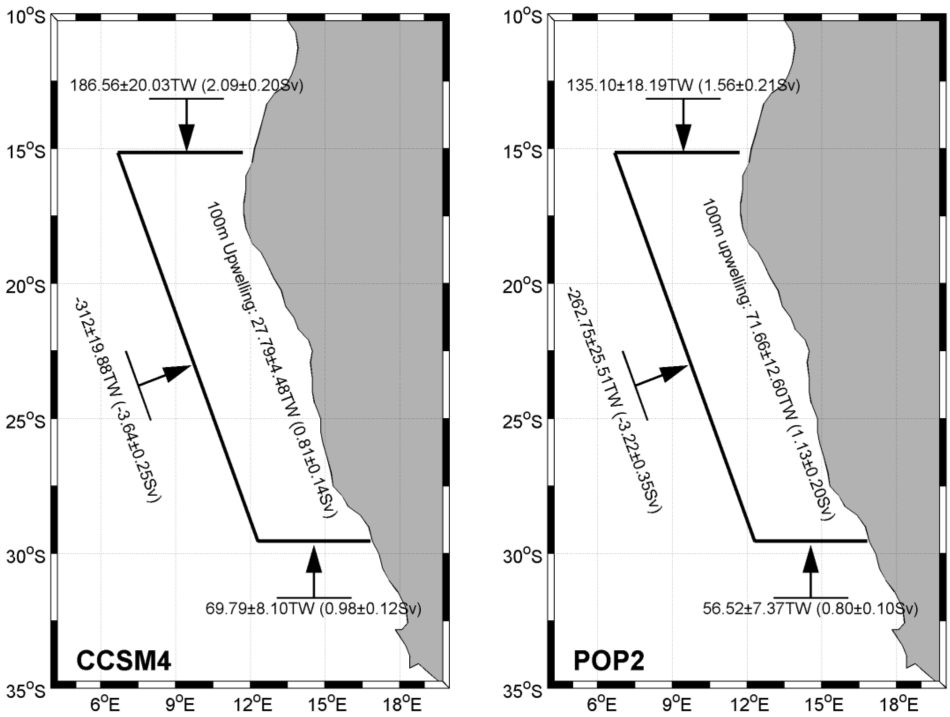

Figure 17 Upper 100m oceanic advection and convection heat transport and volume transport in the BC region in (a) CCSM4 and (b) POP2.

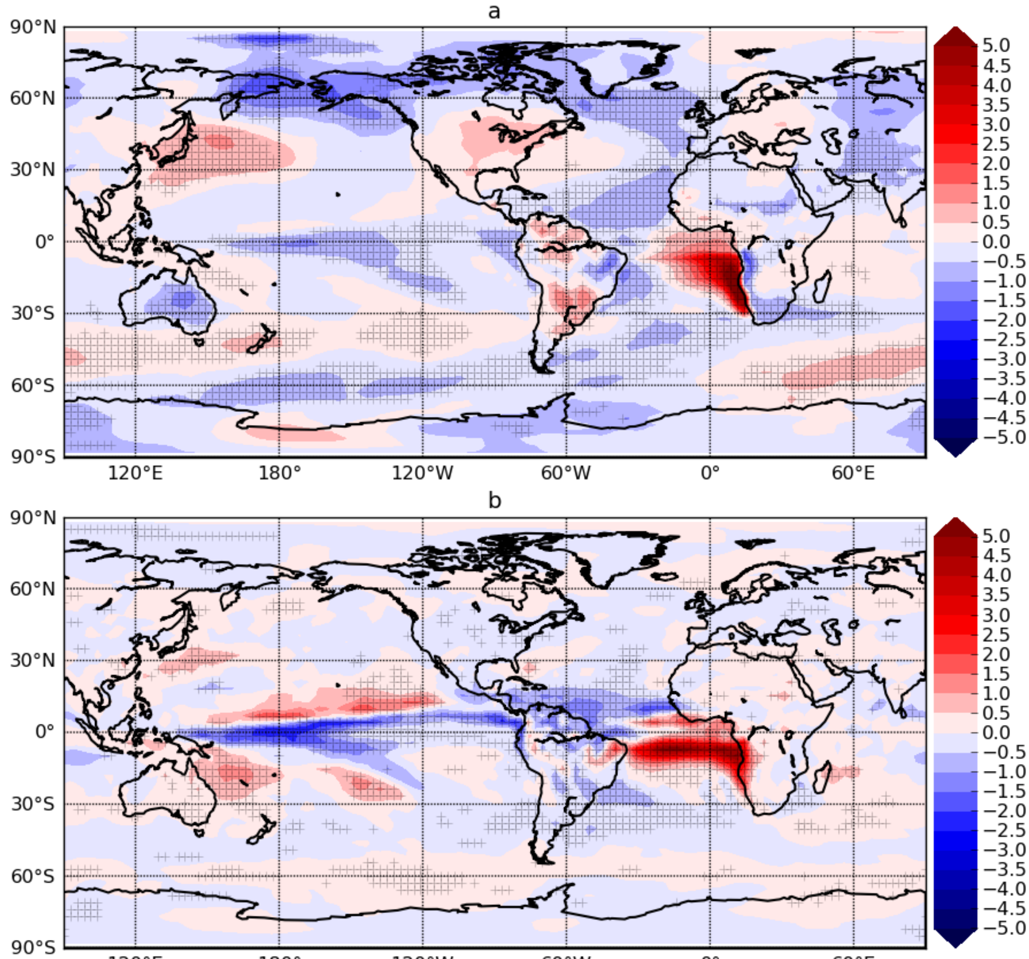

Figure 18 Surface temperature difference (a, in °C) and precipitation difference (b, in mmd^{-1}) between SST-bias run and control run. The regions marked by "+" indicate that the difference is significant at 95% level based a student T-test.